Please cite this article in press as: Morita et al., The Lipid Mediator Protectin D1 Inhibits Influenza Virus Replication and Improves Severe Influenza, Cell (2013), http://dx.doi.org/10.1016/j.cell.2013.02.027

Cell

The Lipid Mediator Protectin D1 Inhibits Influenza Virus Replication and Improves Severe Influenza

Masayuki Morita,[1,14] Keiji Kuba,[1,14] Akihiko Ichikawa,[1] Mizuho Nakayama,[1] Jun Katahira,[2] Ryo Iwamoto,[4,5] Tokiko Watanebe,[6,8,10] Saori Sakabe,[6,10] Tomo Daidoji,[11] Shota Nakamura,[3] Ayumi Kadowaki,[1] Takayo Ohto,[1] Hiroki Nakanishi,[7] Ryo Taguchi,[7] Takaaki Nakaya,[11] Makoto Murakami,[12] Yoshihiro Yoneda,[2] Hiroyuki Arai,[4] Yoshihiro Kawaoka,[6,8,10] Josef M. Penninger,[13] Makoto Arita,[4,9] and Yumiko Imai[1,*]

[1]Department of Biological Informatics and Experimental Therapeutics, Graduate School of Medicine, Akita University, Akita 010-8543, Japan
[2]Biomolecular Networks Laboratories, Biomolecular Dynamics Laboratory, Graduate School of Frontier Biosciences
[3]Department of Infection Metagenomics, Research Institute for Microbial Diseases
Osaka University, Osaka 565-0871, Japan
[4]Department of Health Chemistry
[5]Business-Academia-Collaborative Laboratory, Graduate School of Pharmaceutical Science
[6]Division of Virology, Department of Microbiology and Immunology and International Research Center for Infectious Diseases, Institute of Medical Science
[7]Department of Metabolome, Graduate School of Medicine
University of Tokyo, Tokyo 113-0033, Japan
[8]ERATO Infection-induced Host Responses Project
[9]PRESTO
Japan Science and Technology Agency, Saitama 332-0012, Japan
[10]Influenza Research Institute, University of Wisconsin-Madison, Madison, WI 53711, USA
[11]Department of Infectious Diseases, Kyoto Prefectural University of Medicine, Kyoto 602-8566, Japan
[12]Biomembrane Signaling Project, Tokyo Metropolitan Institute of Medical Science, Tokyo 156-8506, Japan
[13]IMBA (Institute of Molecular Biotechnology in the Austrian Academy of Sciences), Vienna 1030, Austria
[14]These authors contributed equally to this work and are co-first authors
*Correspondence: imai@med.akita-u.ac.jp
http://dx.doi.org/10.1016/j.cell.2013.02.027

SUMMARY

Influenza A viruses are a major cause of mortality. Given the potential for future lethal pandemics, effective drugs are needed for the treatment of severe influenza such as that caused by H5N1 viruses. Using mediator lipidomics and bioactive lipid screen, we report that the omega-3 polyunsaturated fatty acid (PUFA)-derived lipid mediator protectin D1 (PD1) markedly attenuated influenza virus replication via RNA export machinery. Production of PD1 was suppressed during severe influenza and PD1 levels inversely correlated with the pathogenicity of H5N1 viruses. Suppression of PD1 was genetically mapped to 12/15-lipoxygenase activity. Importantly, PD1 treatment improved the survival and pathology of severe influenza in mice, even under conditions where known antiviral drugs fail to protect from death. These results identify the endogenous lipid mediator PD1 as an innate suppressor of influenza virus replication that protects against lethal influenza virus infection.

INTRODUCTION

Despite immunization programs, influenza A viruses are a major cause of morbidity and mortality throughout the world, especially among individuals with high risk factors, such as diabetes, asthma, or pregnancy (Clark and Lynch, 2011). Highly pathogenic avian H5N1 influenza viruses continue to circulate with mortality rates of up to 60% of infected patients (Beigel et al., 2005). Influenza strains have also recently emerged that exhibit resistance to antiviral drugs such as oseltamivir (Shankaran and Bearman, 2012). Recently, a virus with its hemagglutinin (HA) derived from H5N1 was identified that is transmissible in ferrets, further supporting that H5N1 viruses have pandemic potential (Imai and Kawaoka, 2012). Moreover, currently used antiviral drugs, though beneficial if administered early in the disease (Kumar, 2011), are not effective in critically ill patients after influenza virus infections (Beigel et al., 2005; Clark and Lynch, 2011; Kumar et al., 2010).

Influenza A viruses are negative-sense RNA viruses that exploit the host cellular machinery for multiple phases of their life cycle (Neumann et al., 2004). Recent genome-wide RNAi screens have identified several host genes and molecular networks crucial for influenza virus replication (Karlas et al., 2010; Hao et al., 2008; König et al., 2010; Shapira et al., 2009).

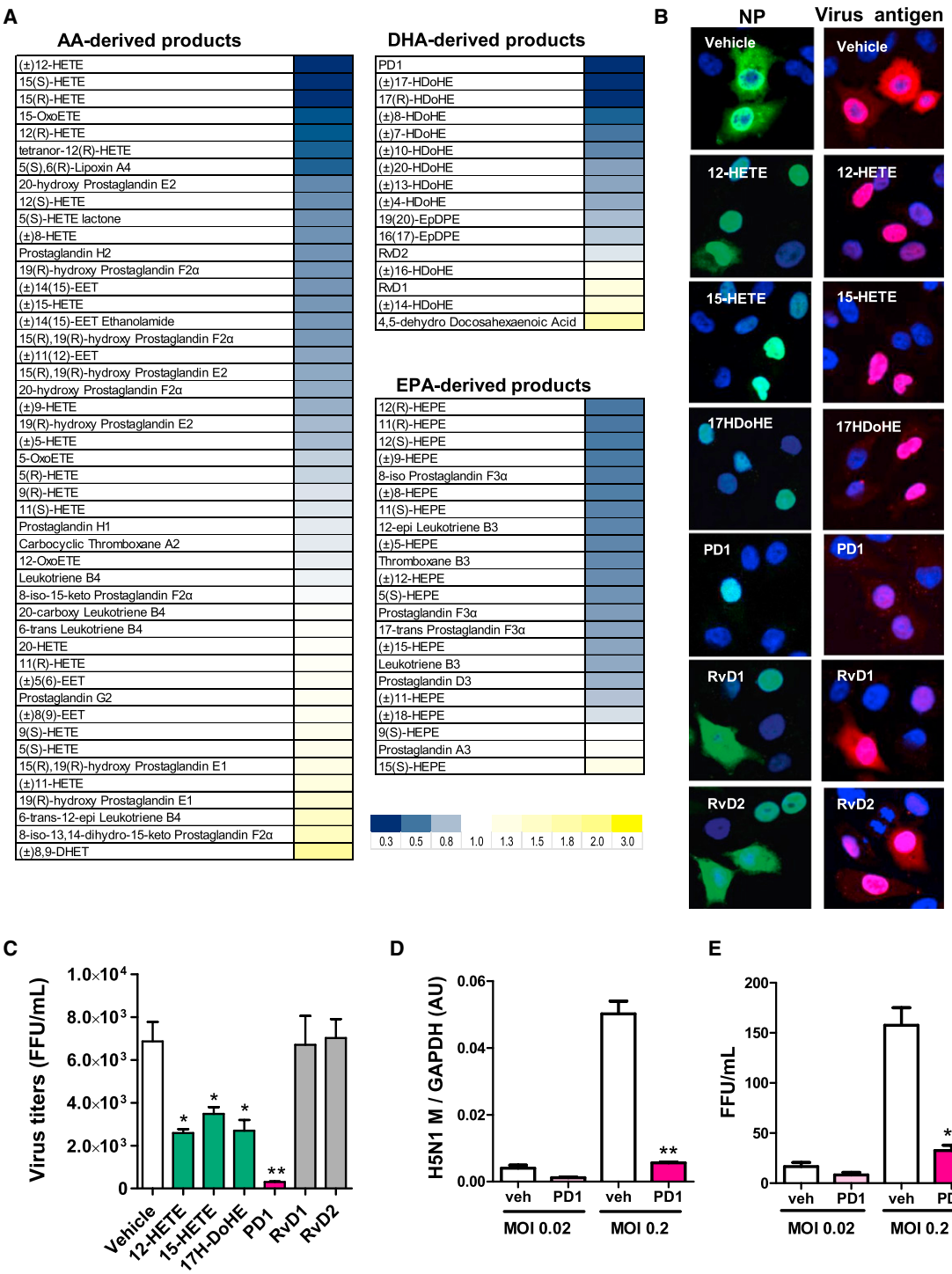

Figure 1. Identification of PUFA-Derived Products Involved in Influenza Virus Replication

(A) Lipid library screening for influenza replication. A549 cells were infected with influenza PR8 virus (MOI: 0.2) and treated with PUFA-derived compound (1 μM) or vehicle immediately after infection. Virus NP mRNA expression was analyzed by calculating the relative ratio of the indicated AA-, DHA-, and EPA-derived compounds to vehicle treatment. Averages from three independent screens shown.

(B) Immunocytochemistry of influenza virus nucleoprotein (NP) and virus antigen R309. PR8-virus-infected A549 cells (MOI: 0.2) were treated with the indicated compounds (1 μM each) or vehicle. Infected cells were fixed after a 24 hr postinfection and stained for NP (green) and virus antigen R309 (red). Nuclei (blue) were counterstained with DAPI.

(legend continued on next page)

However, whether bioactive lipid mediators and lipid metabolic pathways might be involved in influenza virus infections is unknown. Omega-3 polyunsaturated fatty acids (PUFA), such as docosahexaenoic acid (DHA) and eicosapentaenoic acid (EPA), both of which are enriched in fish oils, serve as substrates for the production of potent bioactive anti-inflammatory lipid mediators, such as resolvins, protectins, maresins, and their biosynthetic intermediates (Serhan, 2007; Serhan et al., 2012).

Here, we report that the DHA-derived protectin D1 isomer (PD1; 10S, 17S-dihydroxydocosahexaenoic acid) markedly attenuates influenza virus replication via interference with the virus RNA nuclear export machinery. PD1 was identified in self-limited resolving inflammatory exudates in vivo (Serhan et al., 2002), where it regulates the innate local response and stimulates resolution. Production of PD1 was downregulated during severe influenza virus infections, e.g., with H5N1 avian influenza viruses, and inversely correlated with the pathogenicity of different H5N1 virus isolates. Importantly, PD1 treatment improved the survival of influenza-virus-infected mice even at later stages of the disease, when current antiviral therapies are not effective (Arya et al., 2010), suggesting that PD1 could be a novel therapeutic target for the treatment of severe influenza virus infections.

RESULTS

The PUFA-Derived Mediator Protectin D1 Reduces Influenza Virus Replication

To investigate the potential role of lipid metabolites in influenza infections, we performed a screen of PUFA-derived lipids in human lung epithelial (A549) cells infected with the influenza A virus stain A/Puerto Rico/8/34 (H1N1) (PR8 virus) by using bioactive lipid libraries that include prostaglandins (PGs), resolvins, protectins, and other PUFA-derived metabolites (Figure 1A). PR8-infected cells (multiplicity of infection [MOI]: 0.2) were treated with PUFA-derived metabolites (1 μM each) and influenza virus nucleoprotein (NP) mRNA expression was quantified at 8 hr after infection (Figure 1A). Compared with vehicle treatment, the arachidonic acid (AA)-derived products 12-HETE and 15-HETE, as well as the DHA-derived 17HDoHE and PD1, inhibited the expression of NP mRNA by more than 30%. Of note, some compounds, e.g., 8,9-DHET, resulted in increased NP mRNA levels that required further analysis; here, we focus on compounds that can inhibit virus replication because they may represent potential therapeutic targets for influenza virus infection. Immunohistochemistry demonstrated that PD1, 17-HDoHE, 12-HETE, and 15-HETE administration markedly decreased the numbers of cells that were positive for the influenza virus NP protein and viral antigen R309 (Figure 1B). In addition, PR8 virus titers were markedly decreased by the treatment with 12-HETE, 15-HETE, 17HDoHE, and PD1 (Figure 1C). Consistent with the results of our screen, the DHA-derived resolvins RvD1 and RvD2 showed no apparent inhibition (Figures 1B and 1C). Because PD1 treatment among all bioactive mediators tested led to the most potent inhibition of PR8 virus replication, we focused on PD1 for our subsequent studies. We confirmed that PD1 treatment attenuated influenza virus replication, as assessed by NP protein production in PR8-virus-infected A549 cells (Figure S1A available online). NP mRNA expression was inhibited by PD1 treatment in a dose-dependent fashion (Figure S1B). Importantly, PD1 treatment also attenuated the replication of highly pathogenic H5N1 influenza viruses, as assessed by markedly reduced viral M protein mRNA expression (Figures 1D and S1C), and decreased virus titers (Figures 1E and S1D) in A549 and MDCK cells. Thus, our screen for PUFA-derived metabolites identified PD1 as a suppressor of influenza virus replication in cultured cells.

Reduction of Endogenous PD1 Production in Lungs of Mice in Severe Influenza Virus Infection

To examine the metabolic profiles of PUFA-derived metabolites in severe influenza infection in vivo, we conducted a mediator lipidomics for AA-, DHA- and EPA-derived metabolites in lung tissues obtained from wild-type mice subjected to intratracheal PR8-virus infections (Ichikawa et al., 2013). All PR8-infected animals died within 8 days (Figure S2A). NP mRNA expression (Figure S2B) and virus titers (Figure S2C) rapidly increased after infection peaking on day 2. PR8 infections also resulted in markedly impaired pulmonary functions as assessed by tissue resistance and tissue elastance (Figure S2D) (Sly et al., 2003). Histologically, numbers of inflammatory cells were slightly increased in the PR8-infected lungs on day 2, and on day 5 we observed pulmonary edema, hemorrhage, and hyaline membrane formation (Figure S2E). Thus, in line with previous reports (Smith et al., 2011; Ichikawa et al., 2013), intratracheal infection with PR8 influenza viruses induces lung pathologies that closely mimic the symptoms of severe influenza in humans.

To identify the endogenous lipid mediators and pathway metabolites during PR8 infections, lung tissues were obtained from PR8- and mock-infected mice at 6, 12, 24, and 48 hr after infection and subjected to liquid chromatography-tandem mass spectrometry (LC-MS/MS)-based lipidomics analysis. This technology has been recently developed and allows researchers to identify and quantify more than 250 PUFA-derived endogenous lipid mediators and pathway metabolites including prostaglandins (PGs), leukotrienes (LTs), lipoxins (LXs), resolvins, protectins, and other AA-, EPA-, DHA-derived products (Arita, 2012). As shown in Tables S1, S2, and S3, several lipid mediators were detectable in noninfected lungs under baseline control conditions. In particular, cyclooxygenase (COX) pathway products such as PGE2 and 6-keto PGF1α and the 12/15-lipoxygenase (12/15-LOX) pathway metabolites 12-HETE, 15-HETE, and 14-HDoHE were present in the lung tissues of untreated control mice (Tables S1 and S2). Next, we examined

(C) Virus titers. PR8-virus-infected A549 cells (MOI: 5) were treated with the indicated compounds (8 μM each) or vehicle. Infectious virus particles were quantified at 24 hr after infection by focus forming unit (FFU) replication assay. $^{**}p < 0.01$, $^{*}p < 0.05$ compared with vehicle.

(D and E) Effects of PD1 on H5N1 virus replication. H5N1 influenza-virus-infected A549 cells (MOI: 0.02, 0.2) were treated with PD1 (8 μM) or vehicle immediately after infection. Viral M protein mRNA expression (D) and virus titers (E) were quantified at 24 hr after infection by qRT-PCR and FFU assay. $^{**}p < 0.01$ compared with vehicle. Data in (C)–(E) are presented as means ± S.E.M. See also Figure S1.

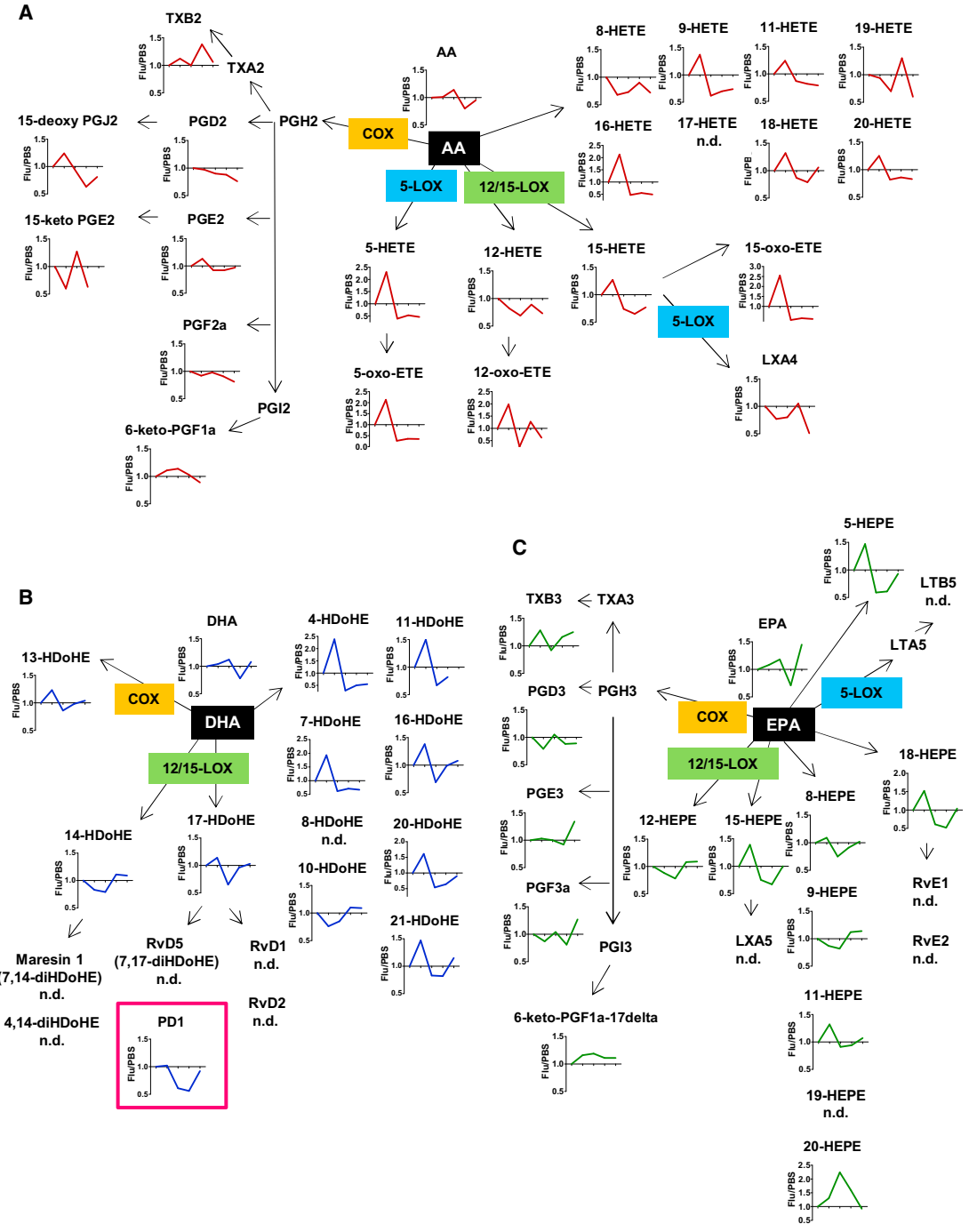

Figure 2. Mediator Lipidomics in Severe Influenza in Mice

(A–C) Lung tissues were obtained from intratracheally PR8 virus (1×10^4 $TCID_{50}$)- or mock (PBS)-infected mice at 0, 6, 12, 24, and 48 hr after infection and subjected to LC-MS/MS lipidomics analysis. Changes in the production of PR8-virus-infected lungs (Flu) relative to PBS-treated controls (PBS) are shown for (A) AA-, (B) DHA-, and (C) EPA-derived metabolites at 0, 6, 12, 24, and 48 hr after infection. n = 5 per each group. See also Figure S2, Tables S1, S2, and S3.

the relative ratios of AA-derived (Figure 2A), DHA-derived (Figure 2B), and EPA-derived (Figure 2C) metabolites in PR8-infected versus control lungs. Intriguingly, among all the identified mediators and metabolites, endogenous production of AA-derived 12-HETE and 15-HETE, as well as DHA-derived 17-HDoHE and PD1, showed the greatest level of reduction during

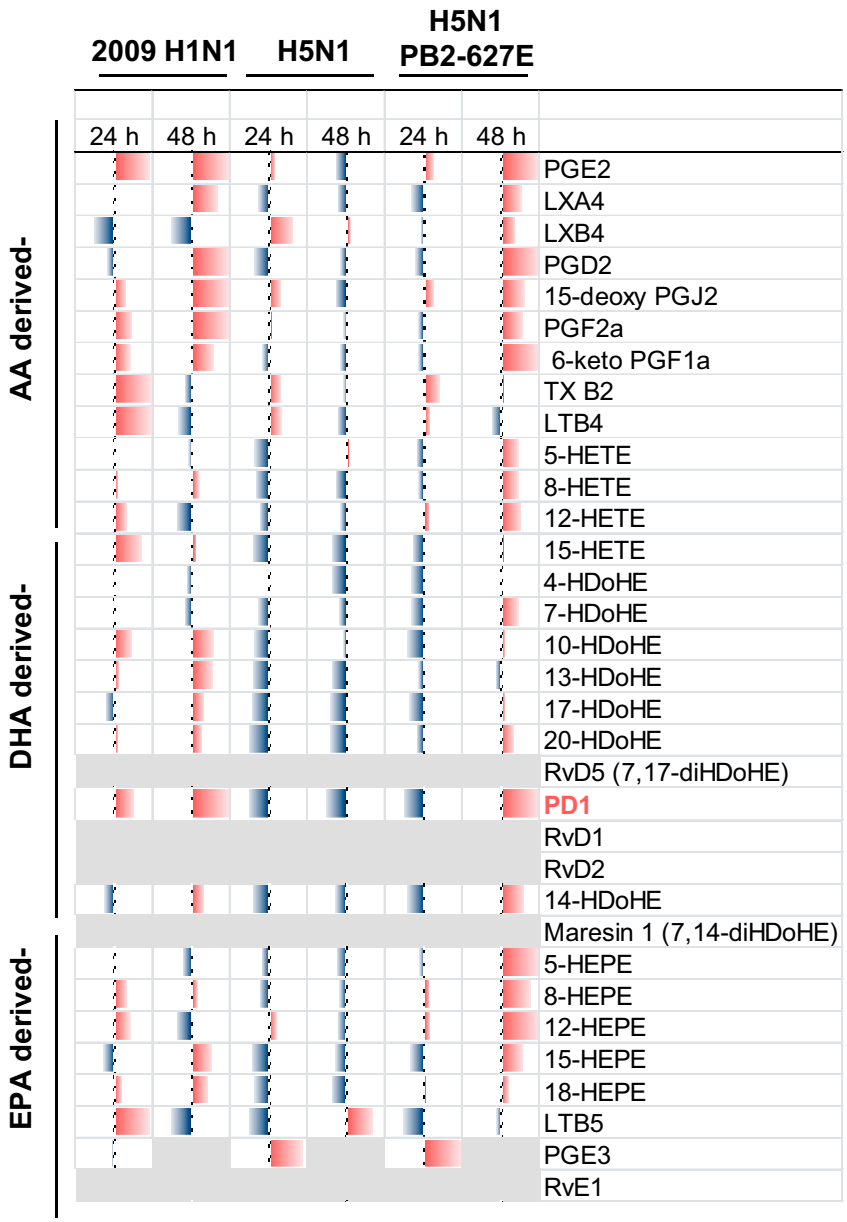

Figure 3. Mediator Lipidomics in H5N1 Influenza Virus Infection in Mice

WT mice were intranasally infected with 2009 H1N1 virus (2009 H1N1), avian H5N1 virus (H5N1), H5N1 virus with an attenuating mutation of Glu at position 627 of PB2 (H5N1 PB2-627E), or mock infected with PBS as a control. Lung tissues were obtained from mice at 24 and 48 hr after infection and subjected to lipidomics analysis. Red columns indicate percent increases and blue columns percent decreases of the indicated lipid mediators in influenza virus (2009 H1N1, H5N1, H5N1 PB2-627E)-infected lungs as compared to PBS-treated controls. Grey columns indicate that the products were not detectable. n = 3 per group.

the course of the PR8 influenza virus infection (Figures 2A–2C); these are the same series of lipid mediators that showed the largest impact on influenza replication in A549 cells (Figure 1). Akin to its effects on viral replication in cell culture, PD1 was one of the most reduced lipid mediator in the lungs of PR8-infected mice (Figure 2B).

To extend our results to other influenza virus strains, we intranasally (i.n.) infected wild-type mice with 2009 H1N1 virus, avian H5N1 (H5N1) virus, avian H5N1 virus carrying an attenuating Glu mutation at position 627 of PB2 (H5N1 PB2-627E), or mock infected them. Virus titers were higher in the lungs of mice infected with the avian H5N1 virus as compared to 2009 H1N1 or H5N1-PB2-627E-virus-infected mice (Figure S2F), confirming previous results (Shinya et al., 2004). Lung tissues were obtained at 24 and 48 hr after infection and subjected to LC-MS/MS-based lipidomics analysis. Again, endogenous production of AA-derived 12-HETE and 15-HETE, and of DHA-derived 17-HDoHE and PD1, was markedly downregulated in lungs infected with the highly pathogenic avian H5N1 virus at both time points analyzed (Figure 3). PD1 production was the most suppressed in H5N1-virus-infected lungs, whereas it was even elevated in lungs infected with the less pathogenic 2009 H1N1 virus and H5N1 PB2-627E virus strains (Figure 3), suggesting that endogenous PD1 levels inversely correlate with the pathogenicity of influenza virus strains. Taken together, our data show that endogenous production of PD1 is markedly suppressed in the lungs of mice intratracheally infected with PR8 virus or nasally infected with the highly pathogenic avian H5N1 influenza virus.

PD1 Protects against Severe Influenza In Vivo

We next tested whether the PUFA-derived 12-HETE, 15-HETE, 17-HDoHE, and PD1, all of which attenuated virus replication in cultured cells (Figure 1), could also protect against severe influenza in mice. Mice were infected intratracheally with PR8 virus (1,500 $TCID_{50}$); lipids mediators (1 μg/mouse) or vehicle were given intravenously (i.v.) 12 hr before and immediately after the PR8 virus infection. The lipids metabolites were given intravenously because they are autacoids and, as such, are rapidly metabolized and inactivated in vivo. Consistent with our in vitro data, PD1 treatment improved the survival of PR8-infected mice (Figure 4A). To extend our results to a human pathogenic virus isolate, we tested whether PD1 treatment could also affect the survival of mice infected with the 2009 H1N1 virus. When PD1 was given i.v. 12 hr before and immediately after 2009 H1N1

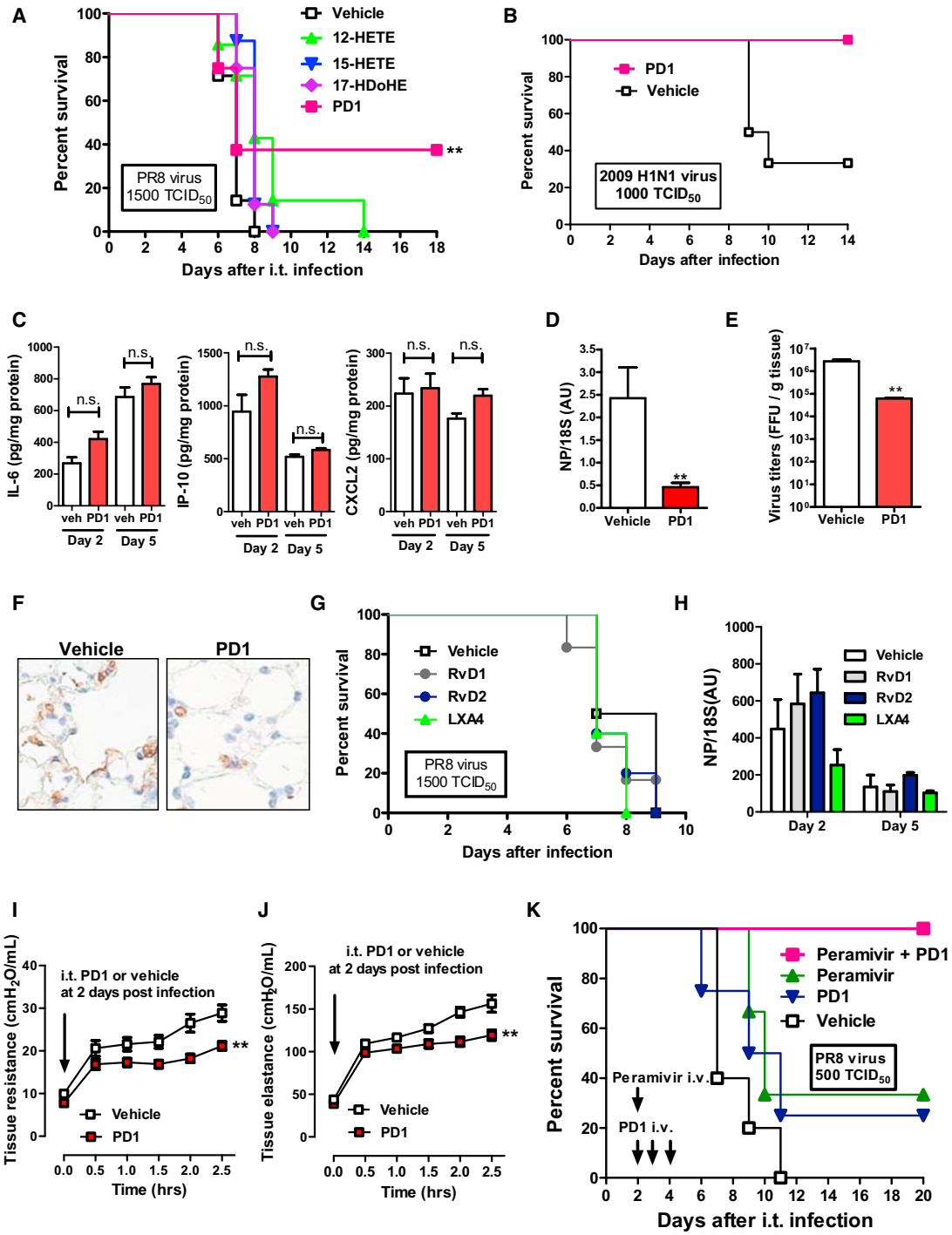

Figure 4. Protective Role of PD1 against Influenza Virus Infection In Vivo

(A) Survival of influenza-virus-infected WT mice upon treatment with PUFA-derived metabolies. n = 7 for vehicle, n = 7 for 12-HETE, n = 8 for 15-HETE, n = 8 for 17-HDoHE, and n = 8 for PD1 group. **p < 0.01 compared with vehicle.

(B) Survival of WT mice intratracheally infected with 2009 H1N1 virus upon treatment with PD1 (1 μg/mouse) (n = 6) or vehicle (n = 6). PD1 treatment improved the survival of virus-infected mice (p = 0.03).

(C–F) Effects of PD1 on host cytokine levels and viral replication. Cytokine (IL-6, IP-10, and CXCL2) levels in lungs at 2 and 5 days postinfection are shown (C). NP mRNA expression (D) and virus titers (E) were measured in lung 24 hr postinfection. n = 5 per each group. n.s., not significant. **p < 0.01 compared with vehicle.

(F) Lung tissues at 2 days after infection were stained with the R309 antibody to detect influenza virus antigen.

(legend continued on next page)

virus infections, the survival of the virus-infected mice improved (Figure 4B). We then tested whether the protective actions of PD1 resulted from its anti-inflammatory functions in macrophages and neutrophils (Schwab et al., 2007). However, macrophage and neutrophil numbers in bronchioalveolar lavage (BAL) fluid were seemingly unaffected by PD1 treatment in the lungs of PR8 influenza-virus-infected mice (Figure S3A), although the PD1-treated lungs did show slightly improved histological changes at 2 days after infection (Figure S3B). Furthermore, PD1 treatment did not significantly decrease the levels of the proinflammatory cytokines IL-6, IP-10, and CXCL2 nor mRNA expression (IL-6, IFN-β, CXCL1, and CXCL2) in the lungs on days 2 and 5 after PR8 infection (Figures 4C and S3C). In contrast, virus NP mRNA expression (Figure 4D), virus titers (Figure 4E), and the number of virus antigen-positive cells (Figure 4F) were all significantly reduced in the lungs of PD1-treated mice, indicating that PD1 acts on viral replication.

Similar to our in vitro data (Figure 1), intravenous treatment (1 μg/mouse) with RvD1 or RvD2 at 12 hr before and immediately after PR8 virus infection had no apparent effect on the survival of PR8-virus-infected mice (Figure 4G). Because LXA4 showed a mild inhibition of virus replication (Figure 1) and LXA4 production was suppressed during the course of severe influenza (Figure 2A), we also tested the effect of LXA4 on the survival of mice infected with PR8 influenza virus in vivo. However, treatment (1 μg/mouse, i.v.) with LXA4 also had no apparent effect on the survival of PR8-virus-infected mice (Figure 4G). Given that RvD1, RvD2, and LXA4 are known to have anti-inflammatory properties (Serhan and Levy, 2003), we next asked whether they could decrease the inflammatory cytokine production initiated in response to virus infection. However, RvD1, RvD2, or LXA4 treatment did not decrease the proinflammatory cytokine levels (IL-6, IP-10, CXCL2) in the lungs on days 2 and 5 after PR8 infection (Figure S3D). In addition, virus replication, as assessed by NP mRNA, was apparently not affected following treatment with these lipid metabolites (Figure 4H).

We finally examined whether PD1 treatment has a therapeutic benefit after the infection was established. Mice were infected i.t. with PR8 virus and treated with PD1 (100 ng/mouse; i.t.) or vehicle 2 days after the initial infection; infected mice were then mechanically ventilated, mimicking the therapeutic setting for critically ill influenza patients in intensive care units. We chose the 48 hr time point because currently available anti-influenza drugs are thought to be beneficial if administered early after infection but ineffective if administered around 48 hr after infection (Kumar, 2011). Intriguingly, such therapeutic PD1 treatment significantly improved the pulmonary functions of PR8-infected mice as assessed by tissue resistance (Figure 4I) and tissue elastance (Figure 4J). A similar administration regiment using RvD1 or RvD2 did not improve pulmonary functions (Figures S3E and S3F). Importantly, when mice were treated with the antiviral drug peramivir (Arya et al., 2010) or PD1 alone at 48 hr postinfection, 70%–75% of the animals still died within 16 days (Figure 4K). However, PD1 plus peramivir treatment beginning 48 hr after infection completely rescued the mice from death due to the influenza infection (Figure 4K). Of note, if treated with peramivir immediately after infection, all animals survived (Figure S3G). These results show that PD1 has a marked beneficial effect on severe influenza virus infections both prophylactically and, most importantly, therapeutically in vivo.

PD1 Inhibits Nuclear Export of Viral Transcripts

Next, we explore the mechanisms by which PD1 inhibits influenza virus replication. Consistent with our in vivo data (Figures 4C, and S3C), expression of antiviral (IFNβ) or anti-inflammatory (IL-8) cytokines was unaffected by PD1 treatment of influenza-virus-infected A549 cells (Figure S4A), suggesting that PD1 is unlikely to attenuate influenza virus replication through its possible antiviral or anti-inflammatory responses. Thus, we wondered whether PD1 could affect influenza virus replication via controlling virus life cycle. The influenza viral genome consists of negative-sense RNA (vRNA) packaged in viral ribonucleoprotein (vRNP) complexes. vRNA is replicated into cRNA, which serves as the template for vRNA neosynthesis. After the formation of vRNPs in the nucleus, vRNAs are exported to the cytoplasm (Neumann et al., 2004). In addition, an initial round of transcription produces 5′ capped and 3′ poly(A) viral mRNA that is also exported to the cytoplasm. To examine whether PD1 affects the nuclear export of influenza virus RNA, we visualized the localization of PR8 virus segment 7 mRNA and vRNA in infected A549 cells using fluorescence in situ hybridization (FISH). Upon PR8 virus infection, virus mRNA and vRNA were primarily localized in the nucleus at 5 hr after infection but shifted to the cytoplasm at 8 hr in the vehicle-treated cells (Figure 5A). PD1 treatment markedly attenuated cytoplasmic translocation of virus mRNA and vRNA (Figure 5A). Of note, RvD1 treatment did not affect the export of viral RNAs (Figure 5A). As a consequence, virus mRNA and vRNA expression was significantly reduced in the PD1-treated but not RvD1-treated cytoplasmic fraction 8 hr after PR8 infections (Figure 5B). Thus, our data indicate that PD1 inhibits nuclear export of influenza virus RNAs.

Genome-wide RNAi screens for host factors implicated in influenza virus replication identified a critical role for the mRNA transporter NXF1 (also known as Tap) (Karlas et al., 2010; Hao et al., 2008), although the precise mechanisms remained unknown. We therefore assessed a potential involvement of

(G and H) RvD1, RvD2, LXA4, or vehicle was given i.v. 12 hr before and immediately after PR8 infection of WT mice (n = 6 for each group). Percent survival is shown (G). NP mRNA expression was measured in lungs at 2 and 5 days postinfection (H).

(I and J) Therapeutic effects of PD1 on lung function of PR8-infected mice. Two days postinfection mice were intratracheally treated with PD1 or vehicle (veh), and then mechanically ventilated for 2.5 hr. Changes in pulmonary tissue resistance (I) and tissue elastance (J) were analyzed. n = 6 per group. $^{**}p < 0.01$ for the entire time course compared with vehicle treatment.

(K) Survival of influenza-virus-infected mice upon delayed treatment with the antiviral drug peramivir (n = 5), PD1 (n = 7), peramivir plus PD1 (n = 7), or vehicle (n = 7). WT mice were infected intratracheally with PR8 virus. In the peramivir group, 2 days postinfection, peramivir (10 mg/kg) was given i.v. In the PD1 group, from 2 days postinfection PD1 (1 μg/mouse/day) was given i.v. for 3 consecutive days. In the peramivir plus PD1 group, peramivir (10 mg/kg) was given i.v. at 2 days postinfection and PD1 (1 μg/mouse/day) was given i.v. for three consecutive days as indicated.

Data in (C), (D), (E), and (H)–(J) are presented as means ± S.E.M. See also Figure S3.

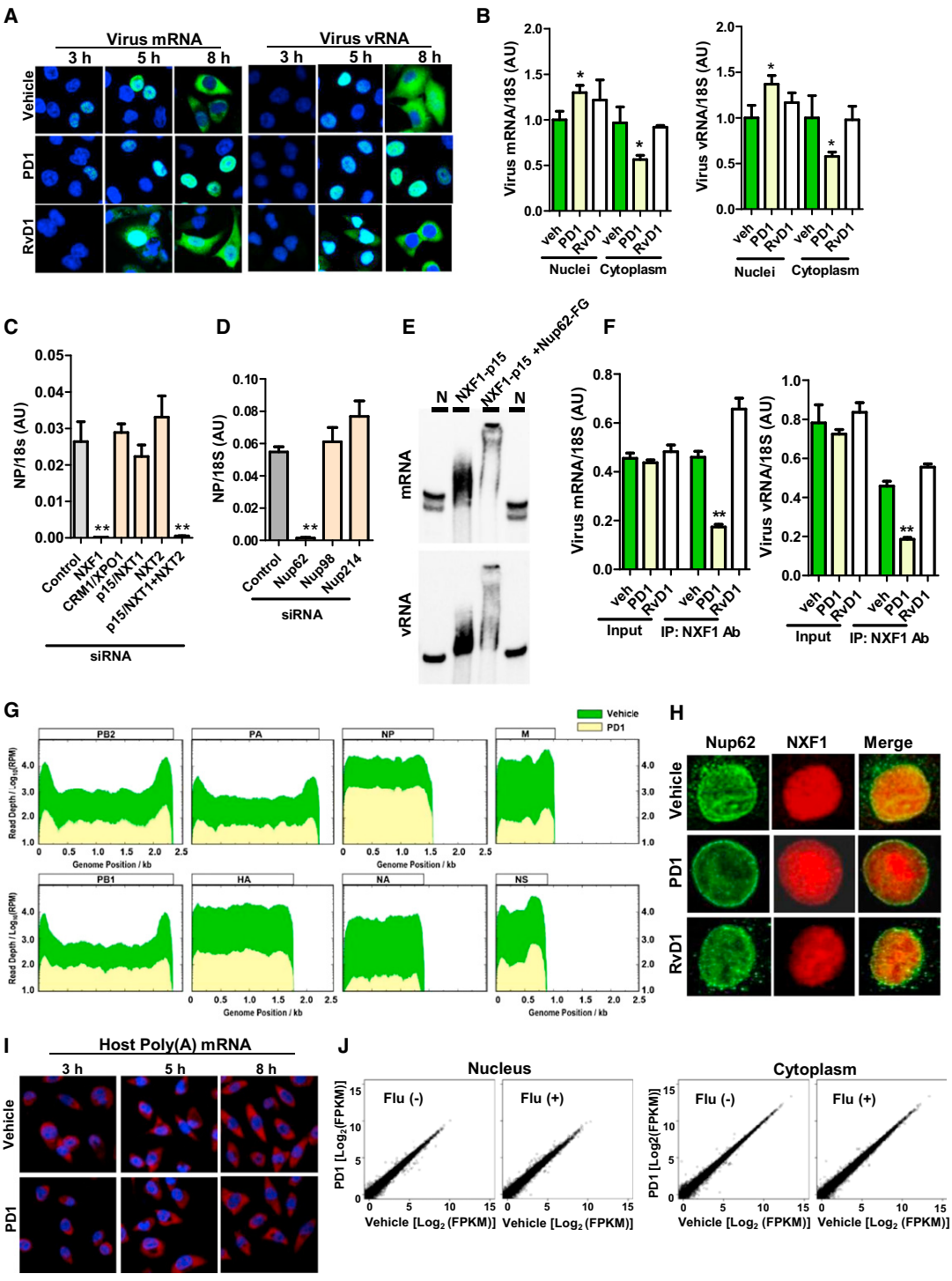

Figure 5. PD1 Inhibits Nuclear Export of Viral Transcripts

(A and B) A549 cells were infected with influenza PR8 virus (MOI: 2) and treated with PD1 (2.7 μM) or vehicle immediately after infection. Infected cells were fixed at the indicated time points, and PR8 virus mRNA and virus vRNA (A) were detected by fluorescence in situ hybridization. Nuclei were counterstained with DAPI. Cytoplasmic and nuclear fractions were separately isolated from the cells at 8 hr after infection, and virus mRNA and vRNA (B) were quantified by qRT-PCR. *$p < 0.05$ compared with vehicle.

(C and D) siRNA knockdown of RNA export genes (C) or FG-nucleoporins (D) in PR8 influenza-infected A549 cells (MOI: 0.2). NP mRNA expression was quantified at 24 hr after infection by qRT-PCR. **$p < 0.01$ compared with control siRNA.

(legend continued on next page)

NXF1 in the PD1-regulated nuclear export of influenza virus RNA. Indeed, knockdown of NXF1 in A549 cells (Figure S4B), but not of the related transporters p15/NXT1 (Herold et al., 2001), NXT2, or CRM1/XPO1 (Stade et al., 1997), significantly attenuated PR8 influenza virus replication as assessed by NP mRNA expression (Figure 5C), NP protein levels (Figure S4C), and virus titers (Figure S4D). Consistent with a previous report (Read and Digard, 2010), FISH analyses further confirmed that knockdown of NXF1 inhibited the nuclear export of virus mRNA and vRNA (Figure S4E). Of note, although knockdown of p15/NXT1 or its homolog NXT2 (Herold et al., 2000) alone did not attenuate virus replication, knockdown of both p15/NXT1 and NXT2 attenuated the influenza virus replication (Figure 5C). Knockdown of CRM1/XPO1 did not affect the nuclear export of influenza virus transcripts (Figure S4F). NXF1 forms a functional heterodimer with the p15/NXT1 protein (Grüter et al., 1998; Herold et al., 2000; Katahira et al., 1999; Rodríguez-Navarro and Hurt, 2011). NXF1 proteins, via their middle (M) and C-terminal domains (Figure S4G), bind to phenylalanine-glycine (FG) repeat-containing nucleoporins (Nups) that line the nuclear pore channel (Ho et al., 2002; Liker et al., 2000). FG-Nups facilitate RNA transport as their repeats provide docking sites for carriers during their movement across the nuclear pore complex (Reed and Hurt, 2002; Stewart, 2010). Among FG-Nups, knockdown of Nup62, but not Nup98 or Nup214, significantly attenuated virus replication assessed by NP mRNA expression (Figure 5D) and virus titers (Figure S5A) in A549 cells, as previously reported for immunodeficiency virus type 1 (HIV-1) infections (Monette et al., 2011). FISH analyses further showed that Nup62 knockdown inhibited the nuclear export of virus mRNA and vRNA (Figure S5B), whereas knockdown of Nup98 nor Nup214 did not affect the nuclear export of influenza virus transcripts (Figure S5C). Whether influenza virus RNAs can directly bind NXF1 has been elusive. By using a cell-free in vitro RNA gel shift assay, we found that recombinant protein expressing full-length NXF1 1-619 and p15/NXT1 (NXF1-p15) generated band shifts of influenza virus mRNA and vRNA (Figure S6A), indicating that influenza virus RNAs directly binds to NXF1-p15. In contrast, we failed to detect a direct binding of Nup62-FG protein to virus RNAs (Figure S6B). Interestingly, coincubation of the NXF1-p15 and Nup62-FG proteins generated a supershift of influenza virus mRNA and vRNA (Figure 5E), supporting the notion that NXF1-p15 and Nup62-FG form a protein complex in vitro, which can bind virus RNAs. Of note, immunoprecipitation experiments showed that Nup62 indeed associated with NXF1 in noninfected and infected cells (Figure S6C). These data indicate that influenza virus RNAs directly bind to NXF1 and that NXF1, in cooperating with a key docking protein Nup62, facilitates influenza virus RNAs export and virus replication.

We next tested whether PD1 could interfere with the recruitment of virus RNAs to NXF1 that can bind Nup62 using an RNA immunoprecipitation (RIP) assays. PD1, but not RvD1, treatment significantly reduced the amount of virus mRNA and vRNA that immunoprecipitated with the anti-NXF1 antibody (Ab) (Figure 5F). The Ab used was immunoprecipitated with NXF1 (Figure S6D). To further confirm this finding, we conducted a RIP sequencing (RIPseq) analysis. The RNAs that immunoprecipitated with the anti-NXF1 Ab indeed mapped to influenza virus RNAs. PD1 treatment significantly reduced the copy number of all influenza virus RNAs that immunoprecipitated with the anti-NXF1 Ab (Figure 5G). Furthermore, we detected the presence of Nup62 microclusters around the nuclear rim and a distinct speckled cytoplasmic staining at 8 hr after infection (Figure 5H). Importantly, upon PD1, but not RvD1, treatment, Nup62 remained at the nuclear envelop in the virus-infected cells (Figure 5H). Taken together, our data indicate that PD1 inhibits the recruitment of virus RNAs to NXF1 that can cooperate with Nup62 for RNA export, thereby attenuating virus RNA export and replication.

Finally, we asked whether PD1 also affects nuclear export of host poly(A) mRNA. FISH analysis showed that PD1 treatment had no apparent impact on the nuclear export of host bulk poly(A) mRNA in the influenza-virus-infected cells (Figure 5I). To confirm this finding, we isolated nuclear and cytoplasmic RNA fractions from the cells at 8 hr after mock or PR8 virus infection and subjected to RNA sequencing (RNAseq) analysis. Consistent with our FISH data (Figure 5I), the distributions of nuclear and cytoplasmic RNA sequences were largely unaffected by PD1 treatment (Figure 5J), although some RNAs appeared changed following PD1 treatment (Table S4); the significance of these changes needs to be determined, though none of these changed RNA have been yet implicated in virus replication.

PD1 Production Is 12/15-LOX Dependent

12/15-LOX (the murine ortholog of human 15-LOX1) (Chanez et al., 2002) is known to be a key enzyme in the biosynthesis of PD1 (Yamada et al., 2011). To test whether the generation of PD1 in the influenza-virus-infected lung was indeed dependent on 12/15-LOX, we conducted lipidomics for PUFA-derived metabolites in 12/15-LOX knockout (KO) (Sun and Funk, 1996) versus control wild-type (WT) mice. Compared with WT mice, levels of PD1 were reduced in 12/15 LOX KO mice at baseline (Figure 6A). Upon influenza virus infection for 24 hr, production

(E) Coincubation of NXF1-p15 plus Nup62-FG proteins generated a supershift of influenza virus mRNA and vRNA. Virus RNA alone (N) served as a negative control.

(F and G) RNA immunoprecipitaion and viral RNA sequencing. Input and immunoprecipitaed RNAs were analyzed by RT-qPCR for virus mRNA and vRNA (F). The immunoprecipitated RNAs were subjected to RNA sequencing. Individual graphs represent the read depth Log10 (RPM) for each segment of the virus (G).

(H) Immunocytochemistry for Nup62 (green) and NXF1 (red) expression in the PD1-, RvD1-, or vehicle treated cells at 8 hr after infection.

(I) The infected cells were fixed at the indicated time points, and Poly(A) mRNA was detected by fluorescence in situ hybridization. Nuclei were counterstained with DAPI.

(J) Host mRNA sequencing. Nuclear and cytoplasmic fractions were isolated from the cells at 8 hr after mock or PR8 virus infection and the extracted RNAs subjected to RNA sequencing. Individual graphs represent the pairwise relationships of the expression level (FPKM) comparing PD1 (y axis) and vehicle (x axis) treatment in nuclear (left) and cytoplasmic (right) RNAs under noninfected and infected conditions.

Data in (B), (C), (D), and (F) are presented as means ± S.E.M. See also Figures S4, S5, S6, and Table S4.

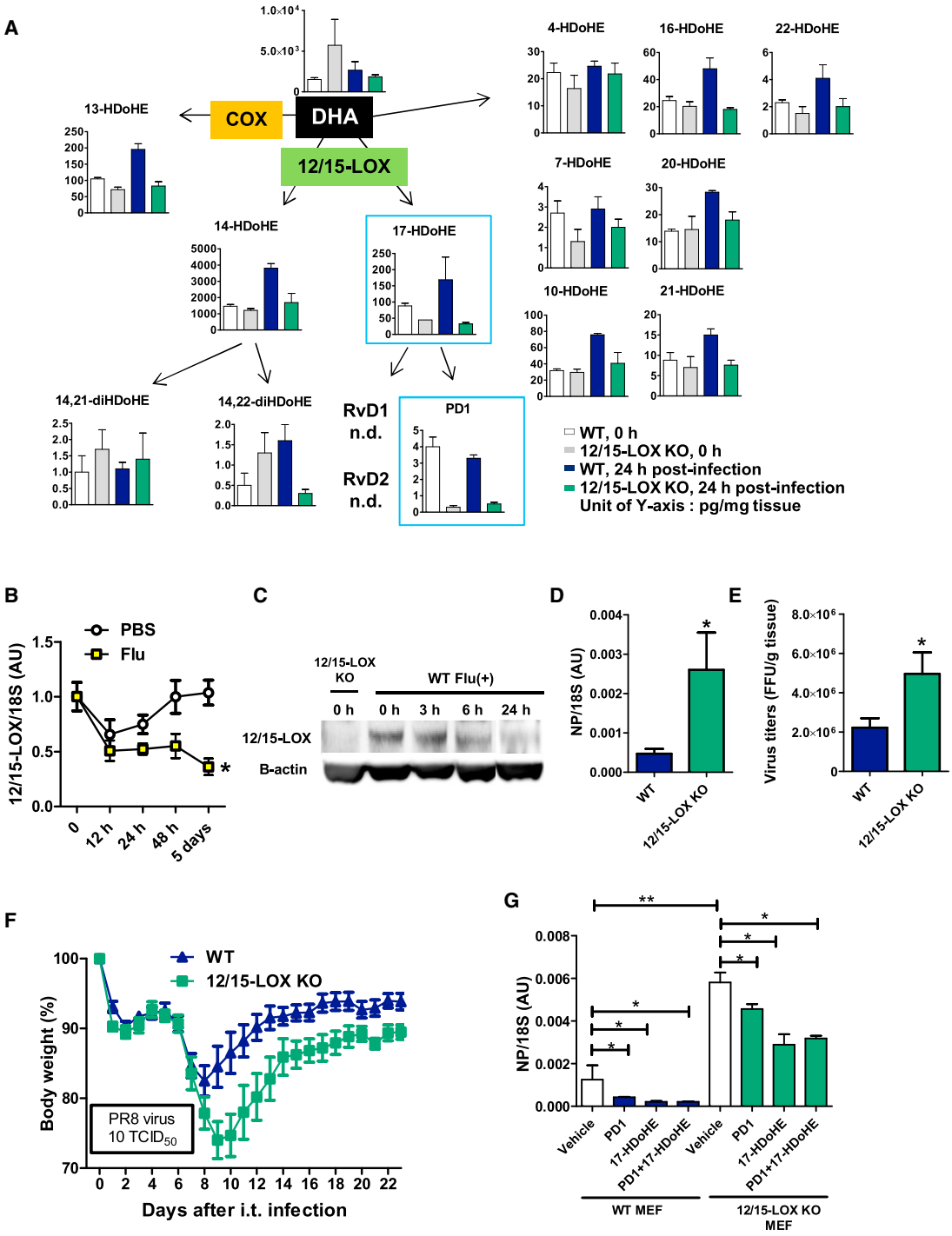

Figure 6. 12/15 LOX-Dependent PD1 Production in Influenza Virus-Infected Lungs

(A) Lipidomics for 12/15-LOX knockout (KO) mice. WT and 12/15-LOX KO mice were infected intratracheally with PR8 virus (1×10^4 $TCID_{50}$). Lung tissues were sampled at time point 0 (baseline) and 24 hr postinfection. The concentrations (pg/mg tissue) of the DHA-derived metabolites are shown; n = 5 per group.

(B) WT mice were intratracheally infected with mock (PBS) or PR8 virus. Lung tissues were sampled at the indicated time points postinfection and 12/15-LOX mRNA levels measured by qRT-PCR. *$p < 0.05$ for the whole time course compared to PBS controls.

(C) Lung tissues were sampled from WT mice at the indicated time points postinfection, and used for western blotting using Abs to 12/15-LOX and β-actin as a loading control. Lung tissues obtained from 12/15 LOX KO mice served as a negative control.

(legend continued on next page)

of PD1 was markedly reduced in 12/15 LOX KO mice (Figure 6A). In addition, the production of 17-HDoHE, the upstream product of PD1, was also markedly reduced in 12/15 LOX KO mice at baseline and at 24 hr postinfection (Figure 6A). Of note, production of LXA_4 was apparently not affected by the genetic inactivation of 12/15-LOX (Figure S7A). 5-lipoxygenase followed by 12-lipoxygenase action (Papayianni et al., 1995) might be involved in the production of lipoxin A4. These data indicate that the endogenous production of PD1 is critically dependent on 12/15-LOX expression.

In lungs, 12/15-LOX is predominantly expressed in epithelial cells and leukocytes (Chanez et al., 2002). In PR8-infected mice, mRNA (Figure 6B) and protein levels (Figure 6C) of 12/15-LOX were decreased in lungs. NP mRNA levels (Figure 6D) and virus titers (Figure 6E) were significantly higher in the lung tissues of PR8-virus-infected 12/15-LOX deficient mice at 2 days postinfection. 12/15-LOX KO mice also exhibited greater body weight loss after PR8 virus infections (Figure 6F). Furthermore, we isolated mouse embryonic fibroblasts (MEFs) from WT and 12/15-LOX KO mice and infected them with the PR8 viruses. NP mRNA levels (Figure 6G) and virus titers (Figure S7C) were again markedly higher in 12/15-LOX KO MEFs. Importantly, the elevated NP mRNA expression (Figure 6G) and virus titers (Figure S7C) in the 12/15-LOX KO MEFs were significantly attenuated by the treatment with PD1, 17-HDoHE, or a combination of both. These results show that the 12/15-LOX is the key enzyme required for the biosynthesis of PD1 and 17-HDoHE in influenza-virus-infected mouse lung.

DISCUSSION

Novel families of biologically active lipid mediators derived from PUFA precursors have recently been uncovered and their complete stereochemical assignments established (Schwab et al., 2007; Serhan, 2007; Serhan et al., 2011; Isobe et al., 2012). These lipid mediators include AA-derived lipoxin A4 (LXA_4), DHA-derived PD1 (also known neuroprotectin D1 when generated in neuronal tissues), D series resolvins (RvD1, RvD2), and the EPA-derived E series resolvins (Serhan, 2007). These mediators are known to have anti-inflammatory properties and display potent protective actions in experimental inflammatory diseases such as peritonitis (Schwab et al., 2007; Yamada et al., 2011) and even Alzheimer's disease (Lukiw et al., 2005). Here, we used mediator lipidomics to show the metabolic profiles and functions of these mediators in the pathology of influenza virus infection. To examine whether such bioactive mediators and biosynthetic intermediates are involved in influenza virus replication, we screened PUFA-derived products for their effects on influenza virus replication. Among them, PD1 markedly attenuated influenza virus replication and, most importantly, promoted survival of infected mice. Similar to PD1, RvD1 and RvD2 are DHA-derived products of the 12/15-LOX pathway (Serhan, 2007). However, RvD1 and RvD2 were under the detection limit after PR8 or H5N1 virus infections, possibly because of scarce infiltration with neutrophils.

The modes of interaction of NXF1 with cellular and viral RNAs are likely to be different. Constitutive transport elements (CTE) of retroviral RNAs can directly bind NXF1 (Braun et al., 1999; Grüter et al., 1998), and NXF1 has been shown to control ICP27-mediated export of Herpes simplex virus (HSV)-1 mRNA (Yatherajam et al., 2011). Although influenza virus infections have been shown to downregulate the host mRNA export machinary by forming an inhibitory complex consisting of viral NS1 and the host NXF1, p15, and other mRNA export factors (Satterly et al., 2007), it was unknown whether NXF1 is in fact involved in the virus RNA export. We show that influenza virus RNAs directly bind to NXF1 and that NXF1, in cooperating with Nup62, facilitates influenza virus RNAs export from the nucleus to the cytoplasm. However, to date it remains largely unknown the involvements of viral proteins and/or adaptor proteins in the NXF1-mediated influenza virus RNAs export (Schneider and Wolff, 2009). Importantly, we found that PD1 attenuates the recruitment of virus RNAs to NXF1 that can bind Nup62 and suppresses the altered localization of Nup62 in the virus-infected cells. The precise mechanisms involved in this process including the PD1's interaction to viral proteins such as NS1 should be clarified in the future study. Furthermore, a yet unidentified specific receptor for PD1 would further raise the important question of how endogenous PD1 controls the downstream pathways connecting to NXF1-Nup62, although PD1 could also have many yet unexplored effects beyond regulation of the nuclear pores.

A key approach to treat severe influenza has been pharmacological targeting of both the virus life cycle and the subsequent extreme pulmonary inflammation. Current anti-influenza virus drugs are beneficial only if administered early after infection; they are much less effective if administered 48 hr after infection (Kumar, 2011). In this context, a key finding of our study is that treatment of PD1 beginning around 48 hr after the initial infection, combined with peramivir, completely rescued mice from flu mortality, indicating that PD1 has a marked beneficial effect on severe PR8 influenza virus infections both prophylactically and, most importantly, therapeutically. Deep RNA sequencing showed that PD1 exhibits only minor effects on host poly(A) mRNA nuclear export under both noninfected as well as infected conditions, although it has not yet identified how PD1 inhibits the export specific for virus RNA rather than host RNA. Antiviral cytokine IFNβ expression levels were also not affected by PD1 treatment in vivo and in vitro. These results may imply that PD1 treatment is not likely to induce a harmful inhibition of host RNA export that could possibly produce detrimental side effects

(D and E) WT and 12/15-LOX KO mice were infected intratracheally with PR8 virus (1×10^4 $TCID_{50}$) Virus NP mRNA (D) and virus titers (E) were quantified in lung tissues at 24 hr postinfection by qRT-PCR and focus forming unit (FFU) replication assay. n = 5 per each group. *p < 0.05 compared with WT.

(F) Body weight changes in influenza-infected 12/15-LOX KO mice. WT (n = 10) and 12/15-LOX KO (n = 11) mice were infected intratracheally with PR8 virus (10 $TCID_{50}$).

(G) Mouse embryonic fibroblasts (MEFs), obtained from WT or 12/15-LOX KO mice, were infected with PR8 virus (MOI: 2) and treated with PD1 (8 μM), 17-HDoHE (8 μM), or a combination of both (4 μM each) immediately after infection. Virus NP mRNA expression was quantified in the infected cells at 24 hr postinfection. **p < 0.01. *p < 0.05. Data in (A), (B), (D), (E), (F),and (G) are presented as means ± S.E.M. See also Figure S7.

in host cells. Given its demonstrated potency, its potent anti-inflammatory properties in sterile and bacterial inflammation (Serhan, 2007), and its production in healthy human airways and reduction in disease (Levy et al., 2007), PD1 could serve as a novel antiviral drug as well as a biomarker for severe and lethal influenza virus infections.

EXPERIMENTAL PROCEDURES

Viruses

A/Puerto Rico/8/34 (H1N1; PR8), A/California/04/2009 H1N1 (2009 H1N1), A/Vietnam/1203/04 H5N1 (H5N1), and a mutant H5N1 virus possessing a single amino-acid substitution, from lysine to glutamic acid, at position 627 in PB2 (H5N1 PB2-627E) were used. BSL3 conditions were used for experiments with H5N1 and H5N1 PB2-627E viruses.

Animals

C57BL/6 mice were bred at our animal facility. 12/15-LOX deficient mice on the C57BL/6 background were purchased from the Jackson Laboratory. Animal experiments and housing of mice were performed in accordance with institutional guidelines.

Intratracheal Influenza Virus Infection Model and Measurements of Respiratory Function

Mice were intratracheally infected with influenza viruses as described elsewhere (Ichikawa et al., 2013). For respiratory function, airway elastance and resistance were measure as described elsewhere (Imai et al., 2005, 2008) using the flexiVent system (SCIREQ).

Mediator Lipidomics

LC-MS/MS-based lipidomics analyses were performed using an high-performance liquid chromatography (HPLC) system (Waters UPLC) with a linear ion trap quadrupole mass spectrometer (QTRAP5500; AB SCIEX) equipped with an Acquity UPLC BEH C_{18} column (Waters) as described (Arita, 2012). MS/MS analyses were conducted in negative ion mode, and fatty acid metabolites were identified and quantified by multiple reaction monitoring (MRM).

Lipid Metabolites

The Protectin D1 isomer (PD1, 10S,17S-diHDoHE), RvD1, RvD2, and 15-HETE-d8, LTB_4-d4, and PGE_2-d4 were purchased from Cayman Chemical. To screen for PUFA-derived compounds, we also used the Bio-active screen Lipid II Library (Cayman Chemical).

Virus Infection of Cultured Cells

The A549 human lung epithelial cells, mouse embryonic fibroblasts and Madin–Darby canine kidney cells (MDCK) were washed with PBS and then infected with virus at the indicated MOIs in DMEM 0.1% BSA for 1 hr at 37°C. Cells were then washed and incubated for the indicated time periods at 37°C in Dulbecco's modified Eagle's medium (DMEM) supplemented with 10% FCS.

Immunocytochemistry

A549 cells on glass coverslips were fixed with 4% paraformaldehyde and incubated with anti-NP Abs (ATCC, Hb65), anti-R309 Abs (Itoh et al., 2009), anti-NXF1-C Abs (Katahira et al., 1999), or anti-Nup62 MAbs (BD Transduction Laboratories), and then incubated with appropriate secondary antibodies. Coverslips were mounted with mounting medium containing 4',6-diamidino-2-phenylindole (DAPI). Images were analyzed with a multiphoton laser microscope (A1R MP, Nikon).

Fluorescent In Situ Hybridization

FISH for influenza virus RNAs and poly(A) mRNA was conducted as described previously (Amorim et al., 2007). To generate a digoxigenin labeled positive- or negative-sense RNA probe, we linearized pSPT19-PR8-M plasmid and transcribed it in vitro with SP6 or T7 RNA polymerase, respectively, by using DIG-RNA labeling kit (Roche). A Cy3-labeled oligo (dT) probe was synthesized for poly(A) mRNA FISH. A549 cells were fixed and permeabilized. After 1 hr prehybridization, the cells were hybridized with the RNA probe for 16 hr at 37°C. A digoxigenin labeled probe was detected by indirect immunofluorescence with an antidigoxigenin fluorescein Fab fragment (Roche). Images were analyzed using multiphoton laser microscopy (A1R MP, Nikon).

Cellular Fractionation

Cytoplasmic and nuclear fractions of the cells were segregated by use of a subcellular protein fractionation kit (Thermo Scientific) in the presence of protease inhibitor cocktail (Roche) and RNase inhibitor (Toyobo).

Quantitative Real-Time PCR

RNA was extracted from cells using the RNeasy Mini Kit (QIAGEN, Valencia, CA). First-strand cDNA was synthesized from DNA-free RNA using a Primescript RT reagent kit (Takara). Samples of first strand cDNA were subjected to real-time PCR quantification (Takara) using specific primers for the indicated RNAs with GAPDH or 18S as an internal control. Relative amounts of RNAs were calculated by using the comparative C_T method.

RNA-Binding Protein Immunoprecipitation Assay and RIP Sequencing

RIP was carried out using an immunoprecipitation kit (RIP-assay kit; MBL). Briefly, cells were homogenized and incubated overnight with protein G agarose beads (Thermo) preincubated with an anti-NXF1 Ab (BD Biosciences) or control Ab. RNAs bound to the beads were purified, and qPCR analysis was carried out. For RIP sequencing, immunoprecipitated RNAs were subjected to RNA sequencing analysis using HiSeq2000 (Illumina). The sequencing run yielded ~30 million reads on average for the PD1 and vehicle treatment samples. Low-quality bases in sequencing reads were trimmed, and the trimmed reads were mapped to the influenza genome of the strain A/Puerto Rico/8/34(H1N1) by using Bowtie2 (Langmead and Salzberg, 2012). Read counts were normalized to reads per million reads (RPM).

RNAseq

Nuclear and cytoplasmic fractionated RNAs were subjected to RNA sequencing analysis using HiSeq2000 (Illumina). The sequencing run yielded ~12 million reads on average. The quality-filtered reads were aligned to the human genome hg19 by using TopHat (Trapnell et al., 2009). The relative expression levels (fragments per kilobase per million mapped fragments, FPKM) were calculated using cuffdiff within the software package Cufflinks version 2.0.2 (Trapnell et al., 2010). The software package CummeRbund version 2.0.0 was used to analyze the output data of cuffdiff (Trapnell et al., 2012).

In Vitro RNA-Binding Assay

To generate PR8 M positive-sense mRNA and negative-sense vRNA, linearized pSPT19-PR8-M was in vitro transcribed with SP6 RNA polymerase and T7 RNA polymerase, respectively, by using MEGAscript kit (Ambion), followed by biotinylation using an RNA3′ end biotinylation kit (Pierce). In vitro RNA gel shift assays were carried out using a chemiluminescent RNA electrophoretic mobility gel shift assay (EMSA) kit (Thermo Scientific) following the manufacturer's instructions. RNA-protein complexes were separated by 4% native polyacrylamide gel, electroblotted to hybond N+ membrane, and the bands visualized with streptavidin-horseradish peroxidase conjugate and chemiluminescence.

Statistical Analyses

Measurements at single time points were analyzed by using an unpaired t test or analysis of variance (ANOVA). Time courses were analyzed by repeated measurements (mixed model) of ANOVA. Log-rank tests were performed on Kaplan-Meier survival curves. All statistical tests were calculated using the GraphPad Prism 5.00 program. $p < 0.05$ was considered to indicate statistical significance.

SUPPLEMENTAL INFORMATION

Supplemental Information includes Extended Experimental Procedures, seven figures, and five tables and can be found with this article online at http://dx.doi.org/10.1016/j.cell.2013.02.027.

ACKNOWLEDGMENTS

We thank all members of our laboratories for helpful discussions. We gratefully thank Ms. Michiko Kamio for technical assistance on LC-MS/MS analyses. Y.I. and K.K. are supported by the Funding Program for Next Generation World-Leading Researchers (NEXT Program, JSPS). Y.K. is supported by the "Center of Education and Research for the Advanced Genome-Based Medicine-For Personalized Medicine and the Control of Worldwide Infectious Diseases," by a grant-in-aid for Specially Promoted Research and by the Japan Initiative for Global Research Network on Infectious Diseases from the Ministry of Education, Culture, Sports, Science and Technology, by ERATO (Japan Science and Technology Agency), and by Public Health Service research grants from the National Institute of Allergy and Infectious Diseases. M.A. is supported by a grant-in-aid from the Japan Science and Technology Agency Precursory Research for Embryonic Science and Technology (PRESTO), and a grant-in-aid from the Ministry of Education, Culture, Sports, Science, and Technology of Japan. J.M.P. is supported by IMBA and an Advanced ERC grant by the European Union. H.A. and M.A. are supported in part by the Program for Promotion of Basic and Applied Research for Innovations in Bio-Oriented Industry.

Received: June 7, 2012
Revised: December 8, 2012
Accepted: February 13, 2013
Published: March 7, 2013

REFERENCES

Amorim, M.J., Read, E.K., Dalton, R.M., Medcalf, L., and Digard, P. (2007). Nuclear export of influenza A virus mRNAs requires ongoing RNA polymerase II activity. Traffic *8*, 1–11.

Arita, M. (2012). Mediator lipidomics in acute inflammation and resolution. J. Biochem. *152*, 313–319.

Arya, V., Carter, W.W., and Robertson, S.M. (2010). The role of clinical pharmacology in supporting the emergency use authorization of an unapproved anti-influenza drug, peramivir. Clin. Pharmacol. Ther. *88*, 587–589.

Beigel, J.H., Farrar, J., Han, A.M., Hayden, F.G., Hyer, R., de Jong, M.D., Lochindarat, S., Nguyen, T.K., Nguyen, T.H., Tran, T.H., et al.; Writing Committee of the World Health Organization (WHO) Consultation on Human Influenza A/H5. (2005). Avian influenza A (H5N1) infection in humans. N. Engl. J. Med. *353*, 1374–1385.

Braun, I.C., Rohrbach, E., Schmitt, C., and Izaurralde, E. (1999). TAP binds to the constitutive transport element (CTE) through a novel RNA-binding motif that is sufficient to promote CTE-dependent RNA export from the nucleus. EMBO J. *18*, 1953–1965.

Chanez, P., Bonnans, C., Chavis, C., and Vachier, I. (2002). 15-lipoxygenase: a Janus enzyme? Am. J. Respir. Cell Mol. Biol. *27*, 655–658.

Clark, N.M., and Lynch, J.P., 3rd. (2011). Influenza: epidemiology, clinical features, therapy, and prevention. Semin. Respir. Crit. Care Med. *32*, 373–392.

Grüter, P., Tabernero, C., von Kobbe, C., Schmitt, C., Saavedra, C., Bachi, A., Wilm, M., Felber, B.K., and Izaurralde, E. (1998). TAP, the human homolog of Mex67p, mediates CTE-dependent RNA export from the nucleus. Mol. Cell *1*, 649–659.

Hao, L., Sakurai, A., Watanabe, T., Sorensen, E., Nidom, C.A., Newton, M.A., Ahlquist, P., and Kawaoka, Y. (2008). Drosophila RNAi screen identifies host genes important for influenza virus replication. Nature *454*, 890–893.

Herold, A., Suyama, M., Rodrigues, J.P., Braun, I.C., Kutay, U., Carmo-Fonseca, M., Bork, P., and Izaurralde, E. (2000). TAP (NXF1) belongs to a multigene family of putative RNA export factors with a conserved modular architecture. Mol. Cell. Biol. *20*, 8996–9008.

Herold, A., Klymenko, T., and Izaurralde, E. (2001). NXF1/p15 heterodimers are essential for mRNA nuclear export in Drosophila. RNA *7*, 1768–1780.

Ho, D.N., Coburn, G.A., Kang, Y., Cullen, B.R., and Georgiadis, M.M. (2002). The crystal structure and mutational analysis of a novel RNA-binding domain found in the human Tap nuclear mRNA export factor. Proc. Natl. Acad. Sci. USA *99*, 1888–1893.

Ichikawa, A., Kuba, K., Morita, M., Chida, S., Tezuka, H., Hara, H., Sasaki, T., Ohteki, T., Ranieri, V.M., dos Santos, C.C., et al. (2013). CXCL10-CXCR3 enhances the development of neutrophil-mediated fulminant lung injury of viral and nonviral origin. Am. J. Respir. Crit. Care Med. *187*, 65–77.

Imai, M., and Kawaoka, Y. (2012). The role of receptor binding specificity in interspecies transmission of influenza viruses. Curr. Opin. Virol. *2*, 160–167.

Imai, Y., Kuba, K., Neely, G.G., Yaghubian-Malhami, R., Perkmann, T., van Loo, G., Ermolaeva, M., Veldhuizen, R., Leung, Y.H., Wang, H., et al. (2008). Identification of oxidative stress and Toll-like receptor 4 signaling as a key pathway of acute lung injury. Cell *133*, 235–249.

Imai, Y., Kuba, K., Rao, S., Huan, Y., Guo, F., Guan, B., Yang, P., Sarao, R., Wada, T., Leong-Poi, H., et al. (2005). Angiotensin-converting enzyme 2 protects from severe acute lung failure. Nature *436*, 112–116.

Isobe, Y., Kato, T., and Arita, M. (2012). Emerging roles of eosinophils and eosinophil-derived lipid mediators in the resolution of inflammation. Front Immunol. *3*, 270.

Itoh, Y., Shinya, K., Kiso, M., Watanabe, T., Sakoda, Y., Hatta, M., Muramoto, Y., Tamura, D., Sakai-Tagawa, Y., Noda, T., et al. (2009). In vitro and in vivo characterization of new swine-origin H1N1 influenza viruses. Nature *460*, 1021–1025.

Karlas, A., Machuy, N., Shin, Y., Pleissner, K.P., Artarini, A., Heuer, D., Becker, D., Khalil, H., Ogilvie, L.A., Hess, S., et al. (2010). Genome-wide RNAi screen identifies human host factors crucial for influenza virus replication. Nature *463*, 818–822.

Katahira, J., Strässer, K., Podtelejnikov, A., Mann, M., Jung, J.U., and Hurt, E. (1999). The Mex67p-mediated nuclear mRNA export pathway is conserved from yeast to human. EMBO J. *18*, 2593–2609.

König, R., Stertz, S., Zhou, Y., Inoue, A., Hoffmann, H.H., Bhattacharyya, S., Alamares, J.G., Tscherne, D.M., Ortigoza, M.B., Liang, Y., et al. (2010). Human host factors required for influenza virus replication. Nature *463*, 813–817.

Kumar, A. (2011). Early versus late oseltamivir treatment in severely ill patients with 2009 pandemic influenza A (H1N1): speed is life. J. Antimicrob. Chemother. *66*, 959–963.

Kumar, S., Havens, P.L., Chusid, M.J., Willoughby, R.E., Jr., Simpson, P., and Henrickson, K.J. (2010). Clinical and epidemiologic characteristics of children hospitalized with 2009 pandemic H1N1 influenza A infection. Pediatr. Infect. Dis. J. *29*, 591–594.

Langmead, B., and Salzberg, S.L. (2012). Fast gapped-read alignment with Bowtie 2. Nat. Methods *9*, 357–359.

Levy, B.D., Kohli, P., Gotlinger, K., Haworth, O., Hong, S., Kazani, S., Israel, E., Haley, K.J., and Serhan, C.N. (2007). Protectin D1 is generated in asthma and dampens airway inflammation and hyperresponsiveness. J. Immunol. *178*, 496–502.

Liker, E., Fernandez, E., Izaurralde, E., and Conti, E. (2000). The structure of the mRNA export factor TAP reveals a cis arrangement of a non-canonical RNP domain and an LRR domain. EMBO J. *19*, 5587–5598.

Lukiw, W.J., Cui, J.G., Marcheselli, V.L., Bodker, M., Botkjaer, A., Gotlinger, K., Serhan, C.N., and Bazan, N.G. (2005). A role for docosahexaenoic acid-derived neuroprotectin D1 in neural cell survival and Alzheimer disease. J. Clin. Invest. *115*, 2774–2783.

Monette, A., Panté, N., and Mouland, A.J. (2011). HIV-1 remodels the nuclear pore complex. J. Cell Biol. *193*, 619–631.

Neumann, G., Brownlee, G.G., Fodor, E., and Kawaoka, Y. (2004). Orthomyxovirus replication, transcription, and polyadenylation. Curr. Top. Microbiol. Immunol. *283*, 121–143.

Papayianni, A., Serhan, C.N., Phillips, M.L., Rennke, H.G., and Brady, H.R. (1995). Transcellular biosynthesis of lipoxin A4 during adhesion of platelets and neutrophils in experimental immune complex glomerulonephritis. Kidney Int. *47*, 1295–1302.

Read, E.K., and Digard, P. (2010). Individual influenza A virus mRNAs show differential dependence on cellular NXF1/TAP for their nuclear export. J. Gen. Virol. *91*, 1290–1301.

Reed, R., and Hurt, E. (2002). A conserved mRNA export machinery coupled to pre-mRNA splicing. Cell *108*, 523–531.

Rodríguez-Navarro, S., and Hurt, E. (2011). Linking gene regulation to mRNA production and export. Curr. Opin. Cell Biol. *23*, 302–309.

Satterly, N., Tsai, P.L., van Deursen, J., Nussenzveig, D.R., Wang, Y., Faria, P.A., Levay, A., Levy, D.E., and Fontoura, B.M. (2007). Influenza virus targets the mRNA export machinery and the nuclear pore complex. Proc. Natl. Acad. Sci. USA *104*, 1853–1858.

Schneider, J., and Wolff, T. (2009). Nuclear functions of the influenza A and B viruses NS1 proteins: do they play a role in viral mRNA export? Vaccine *27*, 6312–6316.

Schwab, J.M., Chiang, N., Arita, M., and Serhan, C.N. (2007). Resolvin E1 and protectin D1 activate inflammation-resolution programmes. Nature *447*, 869–874.

Serhan, C.N. (2007). Resolution phase of inflammation: novel endogenous anti-inflammatory and proresolving lipid mediators and pathways. Annu. Rev. Immunol. *25*, 101–137.

Serhan, C.N., and Levy, B. (2003). Novel pathways and endogenous mediators in anti-inflammation and resolution. Chem. Immunol. Allergy *83*, 115–145.

Serhan, C.N., Hong, S., Gronert, K., Colgan, S.P., Devchand, P.R., Mirick, G., and Moussignac, R.L. (2002). Resolvins: a family of bioactive products of omega-3 fatty acid transformation circuits initiated by aspirin treatment that counter proinflammation signals. J. Exp. Med. *196*, 1025–1037.

Serhan, C.N., Krishnamoorthy, S., Recchiuti, A., and Chiang, N. (2011). Novel anti-inflammatory—pro-resolving mediators and their receptors. Curr. Top. Med. Chem. *11*, 629–647.

Serhan, C.N., Dalli, J., Karamnov, S., Choi, A., Park, C.K., Xu, Z.Z., Ji, R.R., Zhu, M., and Petasis, N.A. (2012). Macrophage proresolving mediator maresin 1 stimulates tissue regeneration and controls pain. FASEB J. *26*, 1755–1765.

Shankaran, S., and Bearman, G.M. (2012). Influenza virus resistance to neuraminidase inhibitors: implications for treatment. Curr. Infect. Dis. Rep. *14*, 155–160.

Shapira, S.D., Gat-Viks, I., Shum, B.O., Dricot, A., de Grace, M.M., Wu, L., Gupta, P.B., Hao, T., Silver, S.J., Root, D.E., et al. (2009). A physical and regulatory map of host-influenza interactions reveals pathways in H1N1 infection. Cell *139*, 1255–1267.

Shinya, K., Hamm, S., Hatta, M., Ito, H., Ito, T., and Kawaoka, Y. (2004). PB2 amino acid at position 627 affects replicative efficiency, but not cell tropism, of Hong Kong H5N1 influenza A viruses in mice. Virology *320*, 258–266.

Sly, P.D., Collins, R.A., Thamrin, C., Turner, D.J., and Hantos, Z. (2003). Volume dependence of airway and tissue impedances in mice. J. Appl. Physiol. *94*, 1460–1466.

Smith, J.H., Nagy, T., Barber, J., Brooks, P., Tompkins, S.M., and Tripp, R.A. (2011). Aerosol inoculation with a sub-lethal influenza virus leads to exacerbated morbidity and pulmonary disease pathogenesis. Viral Immunol. *24*, 131–142.

Stade, K., Ford, C.S., Guthrie, C., and Weis, K. (1997). Exportin 1 (Crm1p) is an essential nuclear export factor. Cell *90*, 1041–1050.

Stewart, M. (2010). Nuclear export of mRNA. Trends Biochem. Sci. *35*, 609–617.

Sun, D., and Funk, C.D. (1996). Disruption of 12/15-lipoxygenase expression in peritoneal macrophages. Enhanced utilization of the 5-lipoxygenase pathway and diminished oxidation of low density lipoprotein. J. Biol. Chem. *271*, 24055–24062.

Trapnell, C., Pachter, L., and Salzberg, S.L. (2009). TopHat: discovering splice junctions with RNA-Seq. Bioinformatics *25*, 1105–1111.

Trapnell, C., Williams, B.A., Pertea, G., Mortazavi, A., Kwan, G., van Baren, M.J., Salzberg, S.L., Wold, B.J., and Pachter, L. (2010). Transcript assembly and quantification by RNA-Seq reveals unannotated transcripts and isoform switching during cell differentiation. Nat. Biotechnol. *28*, 511–515.

Trapnell, C., Roberts, A., Goff, L., Pertea, G., Kim, D., Kelley, D.R., Pimentel, H., Salzberg, S.L., Rinn, J.L., and Pachter, L. (2012). Differential gene and transcript expression analysis of RNA-seq experiments with TopHat and Cufflinks. Nat. Protoc. *7*, 562–578.

Yamada, T., Tani, Y., Nakanishi, H., Taguchi, R., Arita, M., and Arai, H. (2011). Eosinophils promote resolution of acute peritonitis by producing proresolving mediators in mice. FASEB J. *25*, 561–568.

Yatherajam, G., Huang, W., and Flint, S.J. (2011). Export of adenoviral late mRNA from the nucleus requires the Nxf1/Tap export receptor. J. Virol. *85*, 1429–1438.

Cell Host & Microbe
Resource

An Atlas of the Epstein-Barr Virus Transcriptome and Epigenome Reveals Host-Virus Regulatory Interactions

Aaron Arvey,[1] Italo Tempera,[2] Kevin Tsai,[2] Horng-Shen Chen,[2] Nadezhda Tikhmyanova,[2] Michael Klichinsky,[2] Christina Leslie,[1,*] and Paul M. Lieberman[2,*]
[1]Computational Biology Program, Memorial Sloan-Kettering Cancer Center, New York, NY 10065, USA
[2]The Wistar Institute, Philadelphia, PA 19104, USA
*Correspondence: cleslie@cbio.mskcc.org (C.L.), lieberman@wistar.org (P.M.L.)
http://dx.doi.org/10.1016/j.chom.2012.06.008

SUMMARY

Epstein-Barr virus (EBV), which is associated with multiple human tumors, persists as a minichromosome in the nucleus of B lymphocytes and induces malignancies through incompletely understood mechanisms. Here, we present a large-scale functional genomic analysis of EBV. Our experimentally generated nucleosome positioning maps and viral protein binding data were integrated with over 700 publicly available high-throughput sequencing data sets for human lymphoblastoid cell lines mapped to the EBV genome. We found that viral lytic genes are coexpressed with cellular cancer-associated pathways, suggesting that the lytic cycle may play an unexpected role in virus-mediated oncogenesis. Host regulators of viral oncogene expression and chromosome structure were identified and validated, revealing a role for the B cell-specific protein Pax5 in viral gene regulation and the cohesin complex in regulating higher order chromatin structure. Our findings provide a deeper understanding of latent viral persistence in oncogenesis and establish a valuable viral genomics resource for future exploration.

INTRODUCTION

Viruses coevolve with their hosts to establish stable and coregulated genomes and gene expression programs (Iyer et al., 2006). DNA tumor viruses are distinguished by their ability to provide a selective growth advantage to host cells and typically establish long-term persistent intracellular infections (Moore and Chang, 2010). Among the most extensively characterized human tumor viruses is Epstein-Barr virus (EBV), which has been implicated as a causative agent in multiple B cell lymphomas, gastric carcinomas, and nasopharyngeal carcinomas (Rickinson and Kieff, 2007; Young and Rickinson, 2004). EBV is estimated to be responsible for ~1% of all human cancers and may also contribute to other disorders, including multiple sclerosis (Ascherio and Munger, 2010; Parkin, 2006). While EBV oncogenes and regulatory pathways have been characterized individually, there have been few studies that examine the network of virus-host interactions at a genomic scale.

Methods emerging from systems biology and functional genomics provide powerful approaches for elucidating these viral-host interaction networks (Aderem et al., 2011). Chronic infection by DNA tumor viruses, such as EBV, is particularly well suited for systems-level interrogation. EBV genomes persist as multicopy DNA episomes in the nucleus of human B lymphocytes (Lieberman, 2006; Lindner and Sugden, 2007), which can be assayed by modern high-throughput sequencing methods. EBV infection of primary human B lymphocytes leads to the efficient establishment of continuously proliferating genetically stable human lymphoblastoid cell lines (LCLs). Additionally, the EBV expression program in LCLs allows for the assay of the full repertoire of viral latency genes, which are able to drive cellular proliferation and survival in vitro and in vivo in immunocompromised hosts (Thorley-Lawson and Gross, 2004). LCLs have also been extensively characterized by human genetic studies, including large-scale consortium projects such as ENCODE and HapMap (Altshuler et al., 2010; Birney et al., 2007), which have created vast repositories of genotype, gene expression, and cellular phenotype data that can be leveraged to better understand host and viral regulatory networks. The contribution of EBV to LCL genome biology and the comprehensive mapping of functional elements of the EBV genome have not been evaluated in these prior studies.

Previous genomics studies of human viruses have been limited in scope, exploring novel virus discovery (Feng et al., 2008), environmental niche characterization (Breitbart et al., 2003; Reyes et al., 2010; Tadmor et al., 2011), in vitro protein interactions (Calderwood et al., 2007; Dyer et al., 2008; Pinney et al., 2009), and small-scale functional genomics. Many of these studies have been done in herpesviruses, such as an RNA-seq analysis of a Burkitt lymphoma cell line (Lin et al., 2010; Xu et al., 2010), a low-density quantitative PCR (qPCR) primer array for chromatin immunoprecipitation (ChIP) on a limited set of host factors (e.g., CTCF and a small set of histone modifications) (Tempera et al., 2010), and ChIP of the viral factors EBNA1(Dresang et al., 2009; Lu et al., 2010) and BZLF1(Bergbauer et al., 2010). There has also been recent exploration of the KSHV epigenome (Günther and Grundhoff, 2010; Stedman et al., 2008; Toth et al., 2010), though it is unclear whether these epigenetic controls are conserved between gammaherpesviruses.

Here, we present a large-scale functional genomic analysis of EBV, which provides insights into viral pathogenesis and B cell

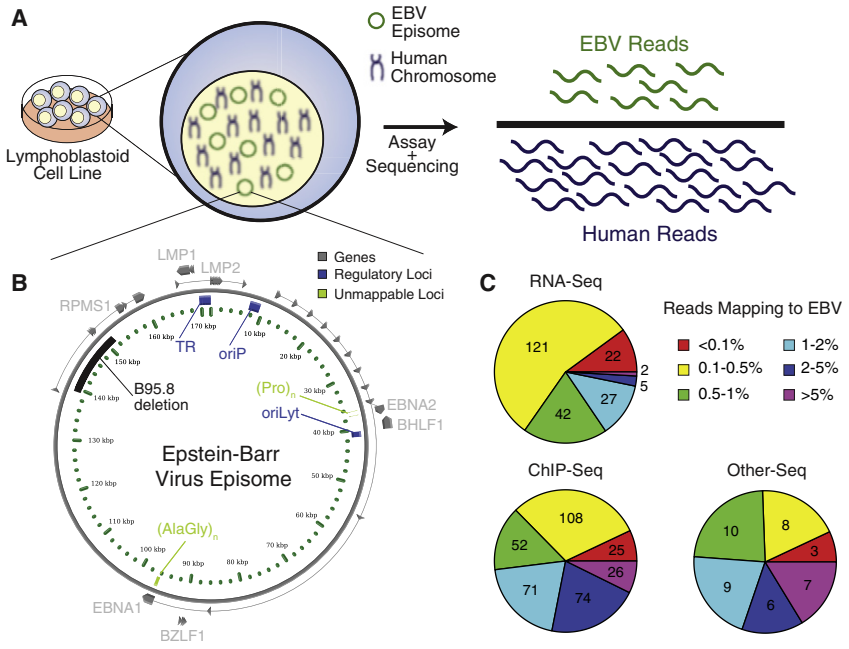

Figure 1. Genomic Profiling of Epstein-Barr Virus in Lymphoblastoid Cell Lines

(A) EBV-infected cell lines were subjected to functional genomics assays coupled with high-throughput sequencing, giving rise to reads that map to the human host and viral genomes.

(B) Known functional elements of the 172 kbp viral episome examined in this study. While we provide all coordinates with respect to the 172 kbp reference, most LCLs were generated with the B95.8 strain, which contains a 12 kbp deletion (139–151 kbp). Unmappable loci have highly similar regions in the human genome, corresponding to reads that are of ambiguous origin.

(C) Short reads from hundreds of ChIP, RNA, and other (DNase, FAIRE, MNase, HiC, etc.) sequencing experiments were mapped to the viral and host genomes. For each experiment, the percentage of aligned viral reads was determined as a fraction of aligned human reads. An average of more than 1% of reads map to the viral genome, though the percentage of viral reads can vary across four orders of magnitude.

EBNA, EBV nuclear antigen; LMP, latent membrane protein; oriP, latent origin of replication; oriLyt, lytic origin of replication; TR, terminal repeats; BHLF1, viral lytic noncoding RNA, BamHI H leftward fragment 1; BHRF1, viral BCL2 homolog, BamHI H rightward fragment 1; BZLF1, viral lytic activating gene, BamHI Z leftward fragment 1; RPMS1, viral gene and promoter for BART miRNAs; RPM, reads per million. See also Figure S1, Table S1, and Table S2.

biology. We integrated our own experimentally generated nucleosome positioning maps and viral protein binding studies with over 700 publicly available high-throughput sequencing data sets for human LCLs that we have mapped to the EBV genome. Many of the cell lines we examined were created by the HapMap Project, and one of these was extensively assayed by the ENCODE Consortium (Altshuler et al., 2010; Birney et al., 2007). Using this massive repository of combined host and virus data, we create a comprehensive atlas of interactions between host factors and the EBV genome. We characterized genome-wide binding profiles of over 60 human transcription factors, which cluster into specific regulatory regions, suggesting combinatorial control of viral gene expression. We discovered host genes that are coexpressed with viral genes and cluster into B cell proliferation pathways. We demonstrated that the host B cell specificity factor Pax5 plays an unexpected role in regulating viral gene expression and chromatin organization. Finally, we characterized the Cohesin-mediated spatial conformation of the viral episome and demonstrate its relevance in gene regulation through knockdown of its structural components. Our study represents a de novo exploration of functional elements and regulators of Epstein-Barr virus on a large scale. All raw and processed data are publicly available at http://ebv.wistar.upenn.edu.

RESULTS

Generating an Atlas of Functional Elements in the EBV Genome

To generate a comprehensive atlas of functional elements for the EBV genome, we analyzed many existing large-scale functional genomics data sets for EBV positive LCLs (Table S1 available online). We examined 319 RNA-seq experiments from five separate studies (Birney et al., 2007; Cheung et al., 2010; Kasowski et al., 2010; Montgomery et al., 2010; Pickrell et al., 2010), covering LCLs from 143 donors, multiple RNA size ranges, cellular compartments and both poly(A)$^+$ and poly(A)$^-$ transcripts. We explored DNA-binding proteins and histone modifications and variants by incorporating more than 300 ChIP-seq experiments from the ENCODE project (Birney et al., 2007). We also integrated cytokine peptide levels (Choy et al., 2008) and related independent functional genomic studies (Lee et al., 2011; Lu et al., 2010; Ramagopalan et al., 2010).

To ensure that we characterized reads of viral origin and excluded reads from homologous human regions, we subtracted reads mapping to the human genome prior to alignment against the EBV genome (Figure 1). This subtraction did not affect mappability of the EBV genome since only a small number of highly repetitive EBV elements are unmappable with reads longer than 24 nucleotides (Figures 1B and S1A–S1D). Alignments to EBV accounted for a significant number of reads in nearly all assays (Figure 1C and Table S2). In total, we aligned over 166 million reads to the EBV genome, which accounted for 1.2% of all mappable reads. As a negative control, we aligned reads from experiments performed in uninfected cell lines and primary tissue and found negligible alignment to EBV (Figures S1E and S1F).

Identification of Regulatory and Transcribed Elements of Epstein-Barr Virus

To explore the overall organization of the functional EBV genome, we summarized viral gene expression, transcription

factor binding, histone modifications, and binding sites of the chromatin insulator CTCF (Figure 2A). An initial overview of the data provided several striking observations.

Viral Regulatory Elements

We identified many candidate regulatory domains of the viral genome that were bound by transcriptional regulators and enriched in histone modifications. We analyzed binding profiles for over 60 human transcription factors, including factors involved in B cell development and viral response, such as Pax5, Irf3, Ebf1, and NFKB. We found that at least 26 transcription factors cumulatively have at least 109 reproducible significant binding sites across the viral genome (Figures 2A and S2A and Table S3). Furthermore, transcription factor binding sites cluster into regulatory loci that are reminiscent of "hotspot" regions identified in other model organisms (Gerstein et al., 2010; Moorman et al., 2006; Roy et al., 2010). Example clusters occurred at promoters for actively transcribed latent transcripts (Cp, RPMS1), as well as at the left lytic origin of replication ($OriLyt_L$). The divergent promoters at $OriLyt_L$ are partitioned into two major clusters of binding factors (Figure 2B). The leftward transcript for BHLF1 has the highest RNA polymerase II peak in the viral genome over its initiation site, which also overlaps with known polymerase cofactors TBP and TAF1. The rightward promoter for BHRF1 (and the associated viral microRNAs [miRNAs]) contains a peak enriched with several factors, including p300, Gcn5, Bcl3, Pbx3, Egr1, Brca1, cFos, and Chd2. We ensured that this locus did not have enrichment for IgG or input DNA sequencing controls and that the overlap was significant (Figures S2B and S2C). The prominent binding of the insulator protein CTCF separates these independent binding sites and their respective divergent promoters, consistent with prior findings (Tempera et al., 2010) (Figures S2D–S2F).

Histone modifications and chromatin boundary factors, like CTCF, are known to contribute to EBV latency regulation but have never been assayed at high resolution (Tempera et al., 2010). The highest measured histone modifications aggregated to a peak at the RPMS1 promoter region, which is the transcription initiation site for a cluster of EBV miRNAs and noncoding RNAs (Figure 2C). CTCF binds downstream of this promoter and appears to serve as a boundary for high-level promoter proximal histone modifications H3K27ac and H3K4me3 (Figure 2C). We also mapped nucleosome positions in two cell lines with different viral latency programs. Nucleosomes strongly occupied the transcriptionally silent Cp promoter in type I Burkitt lymphoma cell lines (which fail to express EBNA2 family genes), while nucleosomes did not occupy the transcriptionally active Cp in type III LCLs (which do express EBNA2 family genes) (Figure 2D). These findings are consistent with reports that active genes have nucleosome-free promoter regions (Zhou et al., 2005).

Viral Transcriptome

The EBV genome is a complex patchwork of densely packed, overlapping, and extensively alternatively spliced genes. As expected in LCLs, the coding and transcribed noncoding domains of the EBV genome were strongly enriched for RNA-seq reads mapping to the latency transcripts for the EBNA genes, latent membrane proteins, and RPMS1, as well as the noncoding RNAs and miRNAs (Table S4). Less expectedly, we detected very high read counts covering the BHLF1 transcript, which is typically associated with early stages of lytic-cycle gene activation and is transcribed from the lytic origin of replication (OriLyt). We also detected other immediate early transcripts such as BZLF1 and BRLF1, though these were expressed at much lower levels. We were also able to verify a recently reported viral-encoded small nucleolar RNA (Hutzinger et al., 2009).

We characterized all RNA splice junctions by analysis of paired end sequencing assays (Table S5). We found many known isoforms and confirmed several recently reported isoforms (Austin et al., 1988; Kelly et al., 2009; Lin et al., 2010). Using deep sequencing from hundreds experiments across multiple labs, we were able to detect dozens of isoforms, including alternative splicing in BZLF1, the BART locus, and multiple 5′ sites that spliced to acceptors in BHRF1 and BHLF1 (Figure 2E). The extensive usage of alternative donor and acceptor splice sites is remarkable and may be relevant for virus regulation and function.

RNA editing occurs in numerous host transcripts and was recently shown to also occur in viral RNAs (Iizasa et al., 2010; Li et al., 2011). Analysis of the many RNA-seq experiments revealed that the BHLF1 RNA transcript contains a guanine nucleotide that differs from the expected adenine residue encoded in the template DNA. This is consistent with classic ADAR-mediated deamination editing (Iizasa et al., 2010). Specifically, ~10% of RNA-seq reads (as averaged across 170 experiments with >10× coverage) mapping to this locus contain the alternative base, whereas only one read in one DNA sequencing experiment (out of n = 26 with >5× coverage) contained this alteration (Figures 2F, S2G, and S2H). BHLF1 RNA has been implicated in the initiation of viral DNA replication, and RNA editing may contribute to this process (Rennekamp and Lieberman, 2011).

Heterogeneity of Viral Gene Expression and Lytic Reactivation in LCLs

In proliferating LCLs, the EBV genome persists predominantly as a type III latent infection, where a limited set of viral genes and miRNAs are expressed and the genome is replicated exclusively by host-cell replication machinery. However, all LCLs contain subpopulations of cells undergoing various degrees of lytic-cycle gene expression and replication, the extent of which varies among cell populations and culture conditions (Davies et al., 2010; Glaser et al., 1989).

We analyzed the EBV gene expression profiles of over 300 LCLs and, after quality filtering, we clustered 201 viral expression profiles (Table S6 and the Supplemental Experimental Procedures). The two main clusters correlated with canonical type III latent and lytic-cycle patterns (Figures 3A and S3). This clustering pattern was stable and consistent across multiple independent labs using independent LCL subclones (Figures 3B and S4). The gene expression clusters correlated with the average EBV load, as measured by the percentage of RNA-seq reads mapping to EBV (Figure 3A, top bar, and Figure S3) and EBV episome copy number as assayed by an independent lab in independent subclones (Figure 3C) (Choy et al., 2008). Since lytic reactivation results in productive replication of the EBV episome, this correlation is an independent validation of lytic activity. However, we also observed disproportionately lower expression of EBV structural and packaging genes associated

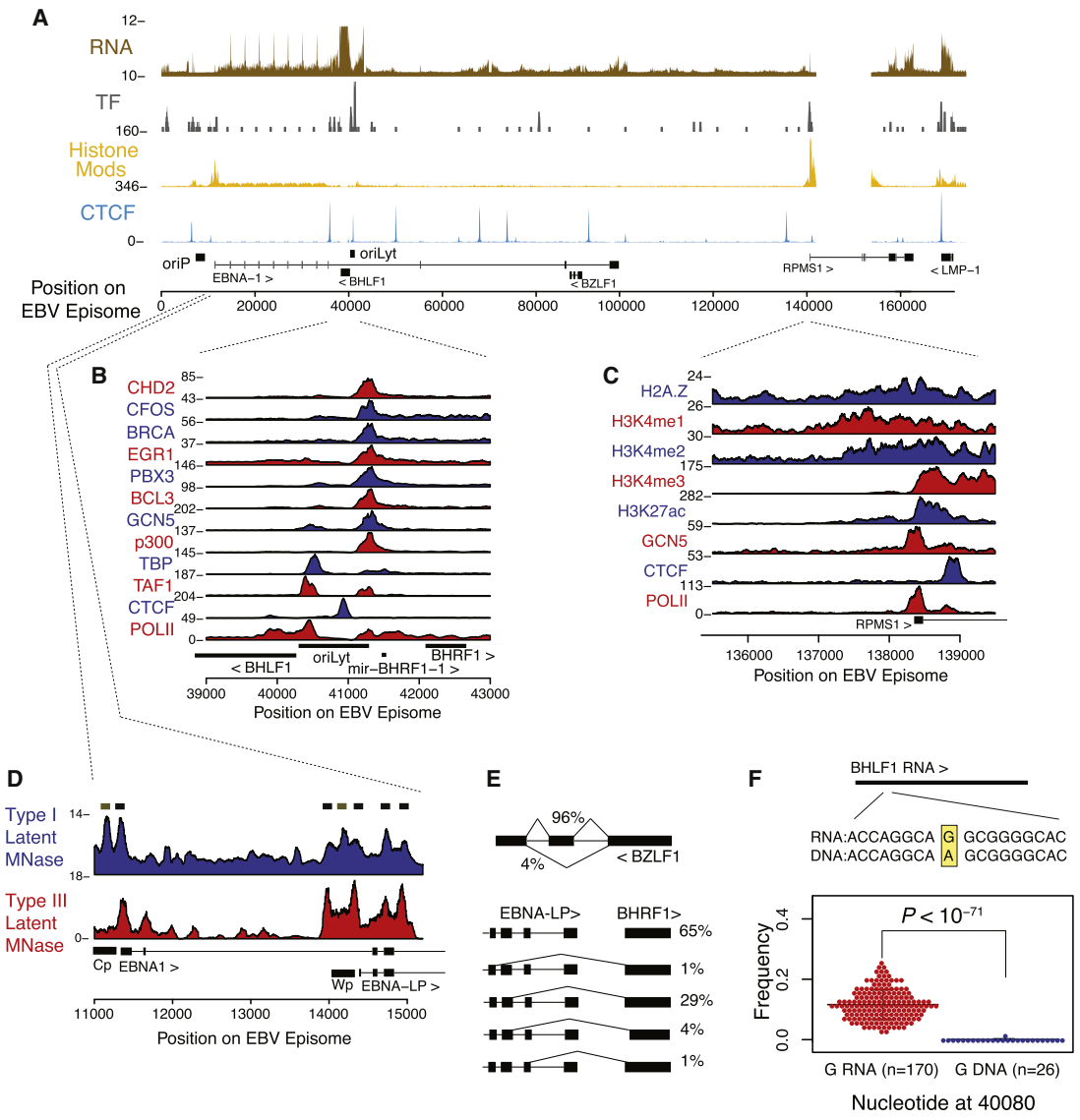

Figure 2. Transcribed and Regulatory Elements of the EBV Genome

(A) The average RNA expression profile (transformed by square root) shows unexpectedly high RNA reads of the lytic cycle-associated transcript BHLF1, in addition to the canonical genes associated with type III latency. Also shown are the number of transcription factor binding sites and average signal of activating histone modifications at known and candidate regulatory regions of the episome. Furthermore, CTCF segments the genome into many more domains than previously recognized.

(B) The lytic origin of replication is highly enriched in transcription factor occupancy. The locus acts as a divergent promoter for the lytic-associated BHLF1 and BHRF1 transcripts separated by a central CTCF binding site.

(C) Histone modifications at the highly transcribed and multiply processed RPMS1 promoter. A peak for H3K4me3 was more proximal, while H3K4me1 was distal to the transcription start site. The histone variant H2A.Z can be seen at the −1 and +1 nucleosomes, and downstream histones are acetylated up to the CTCF site.

(D) Nucleosome occupancy correlates with promoter silencing in different latency types. Nucleosomes have higher occupancy at Cp and Wp in type I latent cells (MutuI), where these promoters are transcriptionally silenced, relative to type III latent cells (LCLs).

(E) RNA-seq reveals transcript isoforms of BZLF1 (top) and EBNA-LP joined to BHRF1 (bottom). The BZLF1 transcript can be alternatively spliced to exclude the coding region for the DNA binding domain, and multiple exons of EBNA-LP can act as donor splice sites to multiple acceptor splice sites in BHLF1. Percentages are given as total of all BZLF1 transcripts and EBNA-LP transcripts, as estimated from reads that cross alternative and canonical splice junctions. BHRF1 is also transcribed canonically from OriLyt.

(F) The BHLF1 RNA transcript differs from the DNA template, suggesting RNA editing by ADAR-mediated deamination. Position 40080 is templated to be an A, but RNA-seq reveals a significant portion of reads across 170 distinct RNA-seq experiments contain a G ($p < 1 \times 10^{-71}$, t test; error bars indicate the SD).

See also Figure S2, Table S3, Table S4, and Table S5.

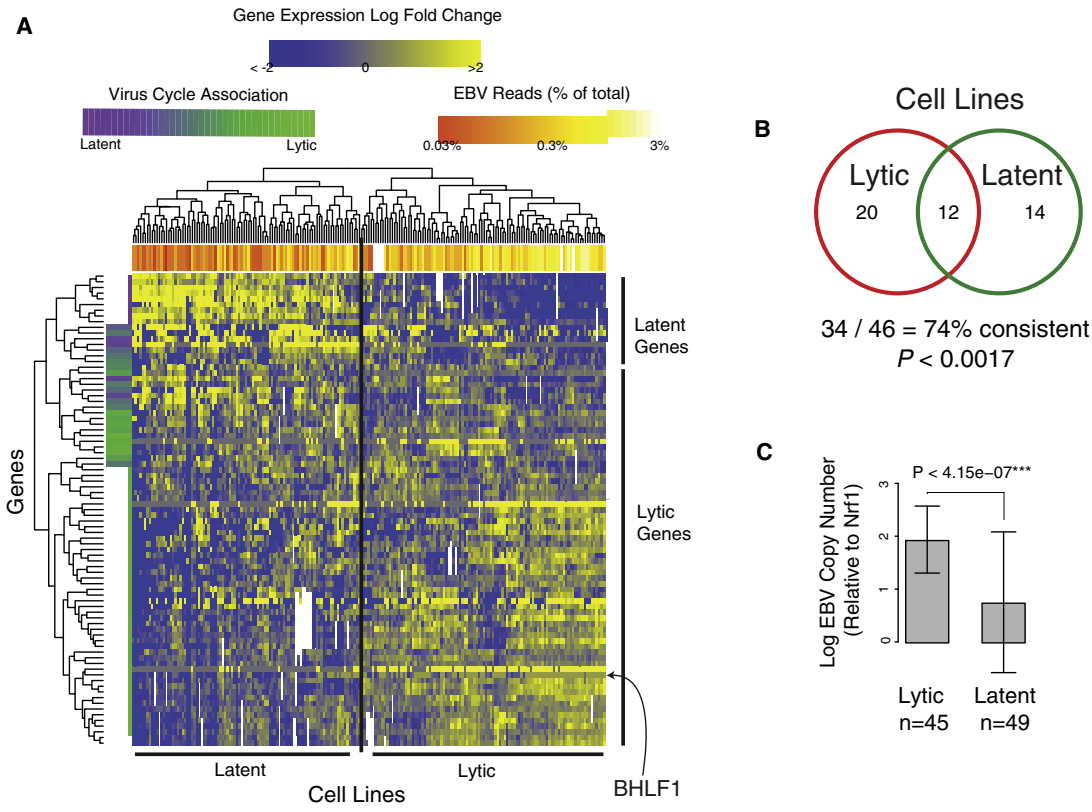

Figure 3. Lymphoblastoid Cell Lines Cluster by Viral Reactivation Propensity

(A) We analyzed gene expression from 201 independent profiles of across 143 lymphoblastoid cell lines and found clustering into type III latency (upper left) or lytic (lower right) gene expression programs. The lytic cluster has a higher percentage of reads mapping to EBV than the latent cluster (bar along top of heatmap). The clustering of genes reveals association with latent and lytic cycle, which is quantified by the first principal component (bar to the left of the heatmap; Supplemental Experimental Procedures). While many of the early-lytic genes are actively expressed, very few of the late-lytic genes required for virion formation are present, suggesting that most reactivation may be abortive.

(B) Propensity for lytic reactivation persists in subclones. Forty-six cell line subclones were assayed in independent labs and have significantly similar latent and lytic viral expression profiles ($p < 0.0017$, binomial test).

(C) EBV copy number, as assayed by qPCR in a separate lab from the RNA-seq experiments, correlates with lytic reactivation clustering and confirms the heritability of expression program.

See also Figure S3 and Table S6.

with infectious virion production (Table S4). This suggests that incomplete or abortive lytic gene reactivation occurs frequently in LCLs.

B Cell Proliferation Pathways Are Coexpressed with Viral Lytic Gene Expression

To better understand the dynamic intracellular environment during viral reactivation, we examined host gene expression and protein levels that correlate with the lytic cycle. We correlated known cellular proteins, metabolic molecules, and surface markers with the latent/lytic state. The cells lines with increased viral lytic cycle tended to have significantly higher ATP, more TNFα, more CCL5, less IL12, and more than double the levels of IL10 (Figures 4A and S4) (Choy et al., 2008). While these molecules are known B cell regulatory factors, their role in lytic reactivation has been less well characterized.

We next used RNA-seq data to simultaneously assay host and viral gene expression and identify cellular gene transcripts that correlate with viral lytic phenotypes (Table S7, Table S8, and Figure S3). LCL RNA-seq was quantified using reads per kilobase of exon per million mapped sequence reads (RPKM) to compute a correlation between EBV lytic gene BHLF1 and human host genes. Many viral genes were expressed at surprisingly high levels relative to human transcripts (Figures 4B and 4C).

We found that EBV lytic gene expression correlated with many human transcripts, for example, the WNT5B transcript (Figures 4D and S4). Searching pathway databases (Subramanian et al., 2005), we found that several families of human genes were significantly correlated with EBV lytic gene expression, including pathways involved in B cell chronic lymphocytic leukemia, interferon-alpha (INFα), WNT, and B cell receptor signaling (Figure 4E, Supplemental Experimental Procedures, and Table S9). An aggregate analysis of all cellular genes bound by the viral transcription factor EBNA1, which is upregulated during lytic reactivation (Figure S4D), revealed a statistically significant increase in virally targeted genes during lytic viral expression, suggesting direct viral regulation of host genes

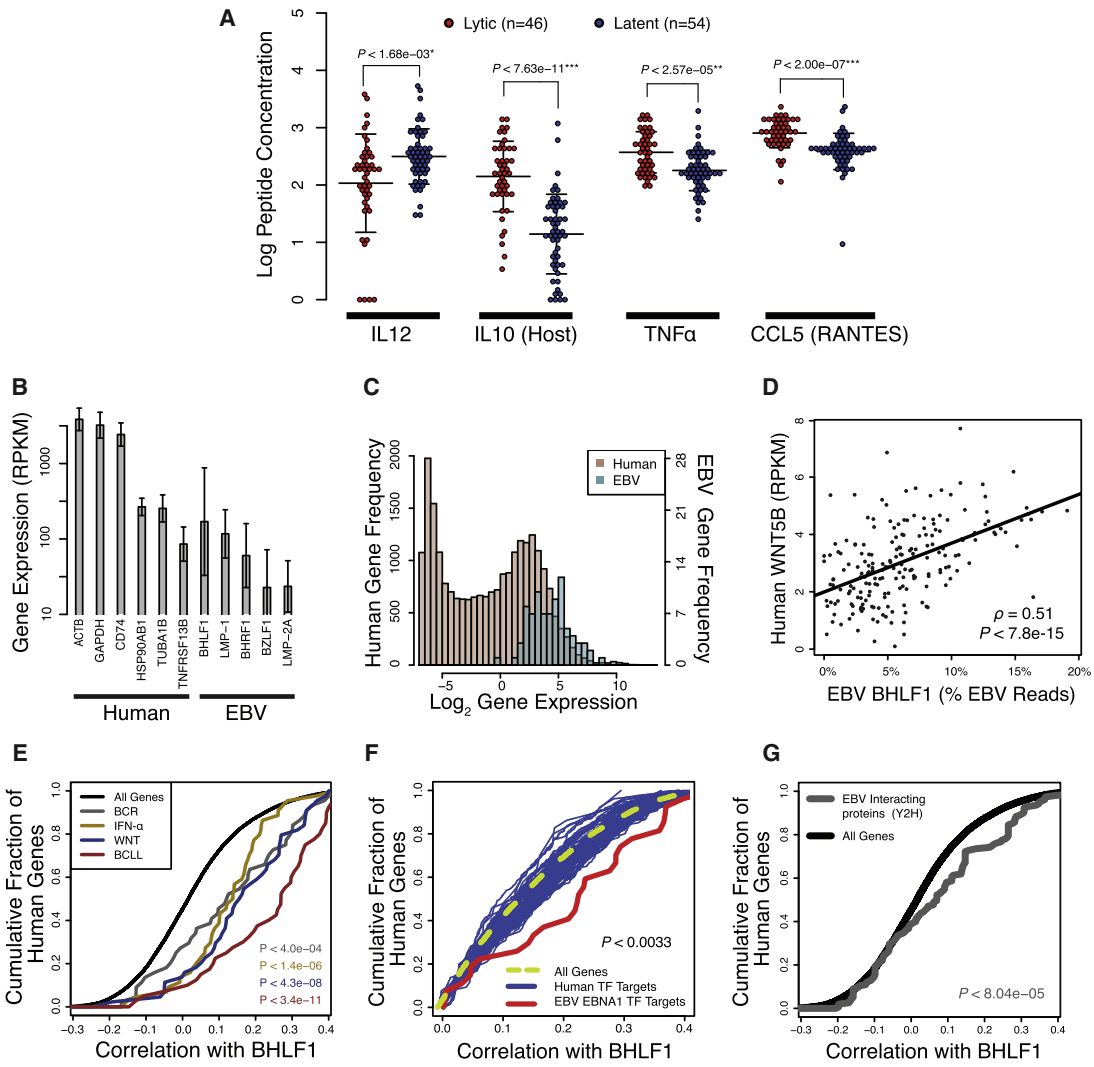

Figure 4. Identification of Host Factors and Genes that Correlate with Spontaneous Lytic Reactivation

(A) Intercellular host cytokine concentrations, as measured by ELISA, are correlated with viral reactivation propensity (Holm corrected p values; error bars indicate the SD).

(B) Specific EBV lytic and latent genes are expressed at similar levels relative to highly expressed human genes (error bars indicate the SD across the 201 samples).

(C) The EBV transcriptome is expressed at similar levels to the human transcriptome.

(D) The human WNT5B gene expression is highly correlated with the EBV lytic reactivation marker BHLF1.

(E) Human genes that correlate with BHLF1 fall into distinct signaling pathways, including B cell receptor (BCR), interferon alpha (IFN-α), Wnt, and B cell chronic lymphocytic leukemia (BCLL) signaling pathways. These pathways represent an amalgamation of EBV-affected alterations and cellular antiviral response mechanisms to increased viral load.

(F) The viral transcription factor EBNA1 (EBV-encoded nuclear antigen 1) binds to genes that are activated during lytic reactivation. Correlation between BHLF1 and ChIP-seq derived high confidence targets of transcription factors is shown.

(G) Host proteins that interact with EBV proteins have their RNA transcripts upregulated during lytic reactivation, as shown by increased correlation with BHLF1.

See also Figure S4, Table S7, Table S8, and Table S9.

(Figure 4F). We also found that cellular genes identified in two-hybrid protein interaction assays with EBV proteins as bait (Calderwood et al., 2007) were correspondingly upregulated with increased lytic gene expression (Figure 4G). Furthermore, we found a small subset of host genes that may be coregulated by multiple means. For instance, the WNT5B gene is bound by EBNA1, is a member of the WNT pathway, and is commonly dysregulated in human cancers, including chronic lymphocytic leukemia (Lu et al., 2004; Lu et al., 2010).

The Host B Cell Lineage Regulator Pax5 Represses Viral Oncogenes

We found that Pax5 binds with high occupancy to the viral terminal repeats (Figure 5), which are known to regulate LMP1 through an unknown mechanism (Repic et al., 2010). Pax5 is

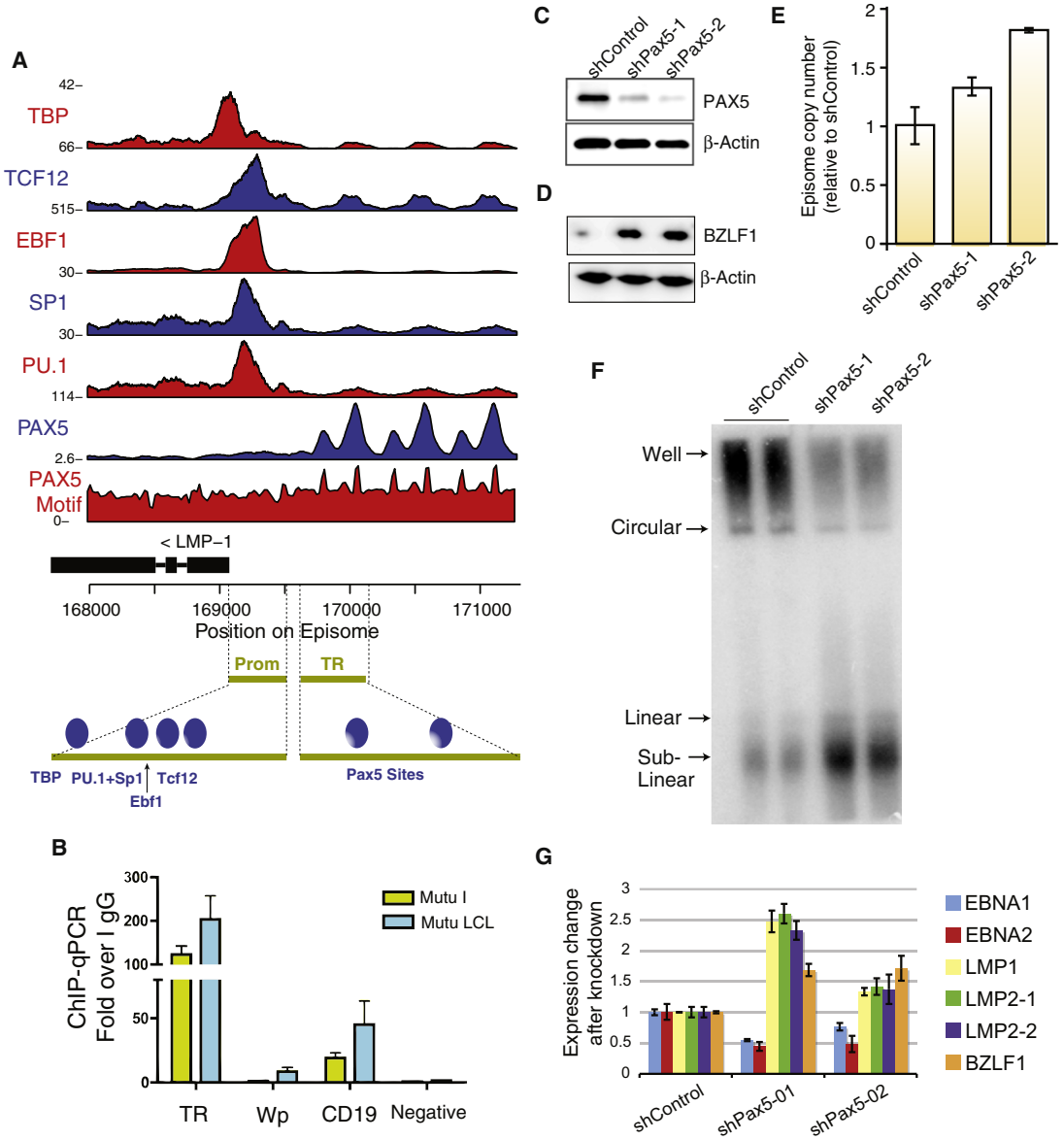

Figure 5. Pax5 Binds the Viral Terminal Repeats and Regulates Viral Oncogene Expression

(A) Pax5 and other transcriptional regulators bind the LMP control region. Pax5 binds the terminal repeats (TR) directly at two sites, as supported by ChIP-seq and sequence motif. In the promoter, EBF1, PU.1, and SP1 were previously documented to cobind a GC-box element and regulate LMP1, while TCF12 has not been reported previously.

(B) Pax5 binds with high occupancy at the TR locus compared with two known binding sites (EBV Wp promoter and human CD19 promoter) as determined by ChIP-qPCR. We also confirm that Pax5 binds the TR in multiple latency types and EBV strains. MUTU presents type I latency and does not express LMP1, whereas MUTU-LCL presents type III latency and expresses LMP1.

(C) Pax5 protein expression is depleted by two independent lentiviral shRNA constructs. Western blot of LCL infected with shPax5-1 or shPax5-2 lentivirus and assayed 5 days after infection followed by puromycin selection.

(D) Western blot of BZLF1 and actin in shPax5-1- or shPax5-2-infected LCLs.

(E) Real-time qPCR analysis of EBV genome copy number relative to cellular actin. Values are normalized to shControl infected LCLs. Error bars indicate the SD from the mean (n = 3).

(F) PFGE analysis of Raji cells infected with shControl, shPax5-1, or shPax5-2 for 5 days after infection and then analyzed by Southern blot analysis. Circular (C), linear (L), and sublinear (SL) forms of the viral genome are indicated.

(G) Knockdown of Pax5 induces LMP1 and LMP2 while decreasing expression of EBNA1 and EBNA2. Pax5 depletion also leads to an increase in the BZLF1 lytic activator. All transcripts are quantified by qRT-PCR and normalized to cellular actin. Error bars indicate the SD from the mean (n = 3).

See also Figure S5.

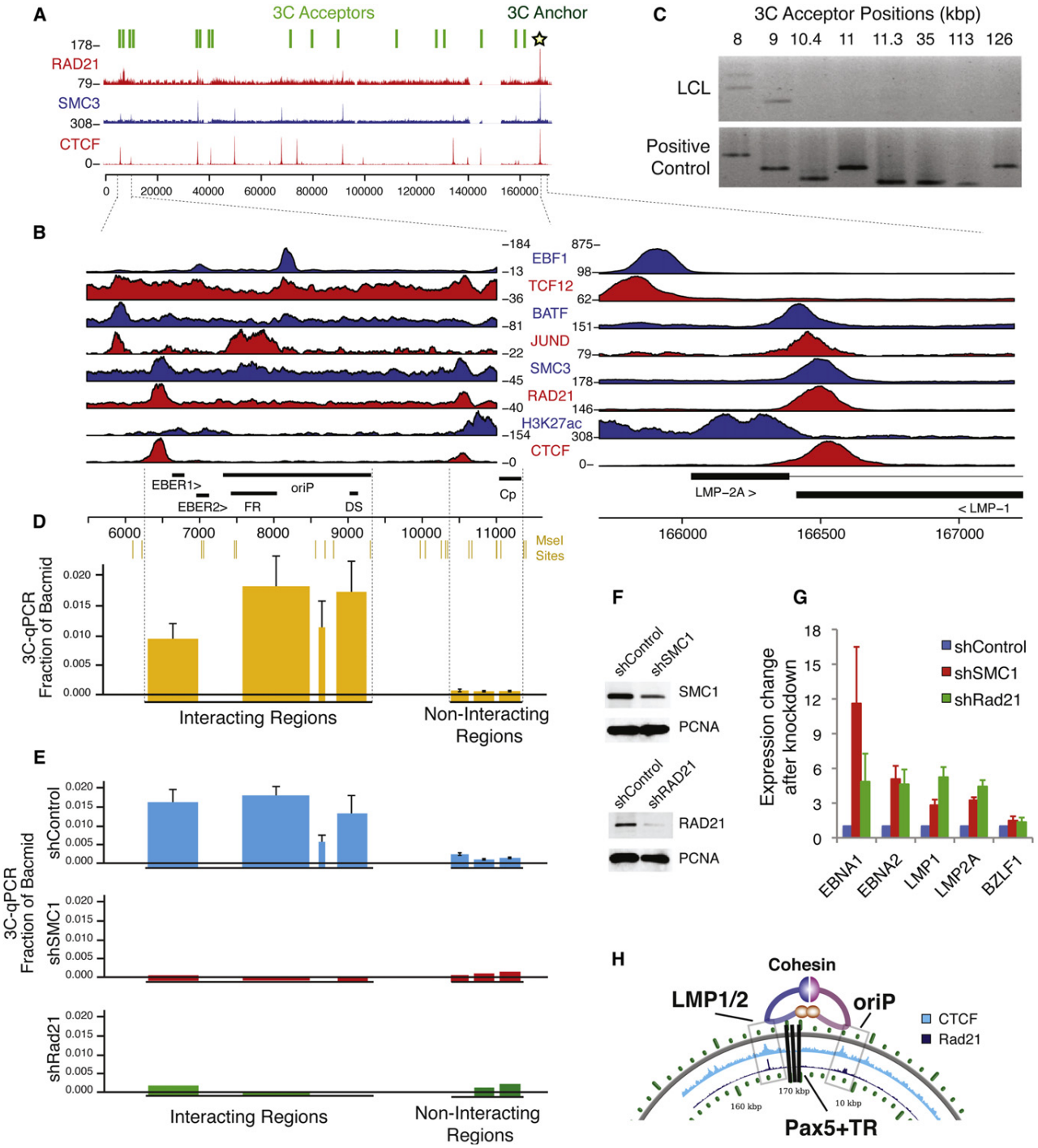

Figure 6. Cohesin Regulates EBV Chromosome Conformation and Latent Cycle Gene Expression

(A) ChIP-seq profiles for chromatin structure protein CTCF and cohesin components (Smc3 and Rad21) demonstrate cobinding at several loci. Chromosome conformation capture (3C) anchor and acceptor primers (shown above) were used to determine DNA loop structures of the viral episome.

(B) Co-occupancy of CTCF, Smc3, and Rad21 at LMP1 and OriP is accompanied by additional transcription factors JUND, BATF, TCF12, and EBF1 and histone modifications.

(C) Identification of a DNA loop between CTCF-cohesin at LMP1 (166.5 kbp) and OriP (~6–9.5 kbp). LCLs (top) subjected to 3C with MseI restriction digestion show specific interaction between oriP and 166.5kbp (anchor). Positive control (bottom) was performed on bacmid ligation products, where all permutations of acceptor sites and anchor are created. The assay is qualitatively specific to under 1 kbp, as shown by the multiple negative regions proximal to OriP.

a B cell-specific factor that plays an essential role in B cell development and contributes to B cell tropism of EBV latency through initial activation of the latency transcription program at Wp (Tierney et al., 2000; Tierney et al., 2007). ChIP-seq analysis reveals two major peaks of Pax5 in at least one, though possibly all, of the viral terminal repeats (Figure 5A). Pax5 binding was validated by real-time PCR with primers specific for terminal repeat (TR) DNA, and a Pax5 consensus motif was identified within the centers of the ChIP-seq peaks (Figures 5A, 5B, and S5A). We also confirmed that Pax5 binds the TR in an alternative EBV strain (Mutu) and in both type I (MutuI) and type III (Mutu-LCL) latently infected cells (Figure 5B). Surprisingly, Pax5 binding at the TR did not overlap with RNA polymerase II initiation factors, suggesting that its function at the TR is more complex than proximal promoter transcription repression. The Pax5 site in the TR is distinct from the known binding sites for Pu.1 and Sp1 in the LMP1 promoter (Sjöblom et al., 1995), which are identified by ChIP-seq along with binding sites for Ebf1 and Tcf12 and are the known sites of EBNA2 transactivation.

To explore the potential function of Pax5 in regulation of EBV gene expression, we depleted Pax5 protein from LCLs using lentivirus-delivered short hairpin RNA (shRNA). We identified two different shRNA targeting sequences that effectively deplete Pax5 protein at 5 days after lentivirus infection and selection (Figure 5C). We first assayed the effect of Pax5 on EBV lytic activation by monitoring BZLF1 protein expression by western blot (Figure 5D) and EBV genome copy number by qPCR (Figure 5E). We found that Pax5 depletion modestly (<2-fold) increased BZLF1 protein expression (Figure 5D) and viral genome copy number (Figure 5E). To assess the effect of Pax5 depletion on EBV genome configuration, we assayed both LCL and Raji cells for circularized and linear viral episomes by pulsed-field gel electrophoresis (PFGE) (Figure 5F). PFGE analysis indicated that Pax5 depletion had only marginal effects on EBV genome copy number in LCL (Figure S5B). In contrast, a percentage of viral episomes were converted to linear and sublinear genomes in Raji cells (Figure 5F). Since Raji are defective for viral lytic replication, these findings suggest that Pax5 may be important for maintaining the circular episomal form of the genome during latency.

To assess the effect of Pax5 depletion on viral transcription, we measured EBV gene expression for LMP1, LMP2 isoform 1 (LMP2-1), LMP2 isoform 2 (LMP2-2), EBNA1, EBNA2, and the lytic immediate early gene BZLF1. We found that Pax5 depletion led to the activation of LMP1 and both isoforms of LMP2 while decreasing EBNA1 and EBNA2 transcript accumulation (Figure 5G). Pax5 depletion also increased BZLF1 transcription, consistent with western blotting results (Figure 5D). These findings indicate that Pax5 contributes to the regulation of EBV transcription during latent infection.

Cohesin Mediates DNA Looping of the Viral Episome

To further explore viral chromosome architecture, we analyzed ChIP-seq binding profiles for the chromatin structural factors CTCF, SMC3, and Rad21 and observed a pattern of colocalization (Figures 6A and S6). Most striking was the strong ChIP signal at the convergence of the LMP1 termination site and LMP2 first intron (Figure 6B). This positioning was highly reminiscent of the CTCF-cohesin site identified within the latency transcript of the KSHV genome (Stedman et al., 2008). Interestingly, Rad21 and SMC3 also colocalized at the origin of latent replication (OriP), which is known to be a central regulatory region for episome maintenance and has been shown to regulate LMP1 through a long-distance enhancer mechanism (Gahn and Sugden, 1995) (Figure 6B).

As CTCF and cohesin have been implicated in long-distance DNA looping interactions, we used the chromatin conformation capture (3C) method to test whether the CTCF-cohesin sites physically linked OriP with the LMP1/LMP2 locus (Supplemental Experimental Procedures and Table S10). Using anchor primers at the LMP1 locus and MseI digestion of the EBV genome, we found a strong 3C linkage formed between the anchor and positions centered around OriP (episome coordinates 6–9 kb) but not at several proximal control regions or other regions across the EBV genome (Figures 6C and 6D). These findings were corroborated by DNA sequencing of the PCR amplified junctions and by use of different primer sets for real time qPCR.

To test whether cohesin subunits have any effect on EBV gene expression, we depleted SMC1 and Rad21 proteins using shRNA. LCLs were infected with lentivirus expressing Rad21 or SMC1 targeting shRNA and assayed by western blot for knockdown efficiency (Figure 6F). Cohesin depletion led to a complete loss of the 3C loop formed between the OriP and LMP1/LMP2 control regions (Figure 6E). qPCR analysis of EBV gene expression revealed that Rad21 or SMC1 depletion resulted in a general increase of latency transcripts, including LMP1 and LMP2 (Figure 6G). Cohesin depletion also led to a modest increase in BZLF1 expression. These results support the model that EBV chromatin forms higher order structures that include loop formation between OriP and the LMP1/LMP2 locus and help maintain viral latent cycle gene expression (Figure 6H).

(D) The long-range interaction is highly robust and specific. 3C-qPCR shows a highly specific quantitative interaction with the region surrounding OriP. The height of the bars represents the qPCR signal relative to positive control bacmid ligation products. The width of the bars demonstrates the size of the MseI restriction enzyme fragment, which is also given at the top of the plot. Error bars indicate the SD from the mean (n = 3).

(E) Depletion of cohesin components through lentiviral shRNA results in loss of long-range interaction. 3C-qPCR was as described in (D), except LCLs were transduced with shControl (top), shSMC1 (middle), or shRad21 (bottom).

(F) Lentiviral shRNA constructs deplete protein expression for Smc1 and Rad21.

(G) Depletion of cohesin components activates transcription of latency genes. Expression of EBNA1, EBNA2, LMP1, LMP2A, and BZLF1 messenger RNA (mRNA) was assayed by qRT-PCR in LCLs infected with shSmc1, shRad21, or shControl. mRNA expression is normalized to shControl. Error bars indicate the SD from the mean (n = 3).

(H) Model depicting a DNA loop between the OriP and LMP loci, which is mediated by CTCF-cohesin binding sites and contains the Pax5 binding sites in the terminal repeats.

OriP, latent origin of replication; FR, family repeats; DS, dyad symmetry repeats; EBER, EBV encoded RNA; Cp, BamHI C promoter. See also Figure S6 and Table S10.

DISCUSSION

Our work integrates large genomic data sets into a comprehensive atlas of functional elements of a human pathogen. We used a strategy of large-scale computational analysis, hypothesis generation, and functional validation to dissect the complex factors implicated in the regulation of both virus and host genes. Our meta-analysis approach also reveals how large-scale projects such as ENCODE and HapMap can have far-reaching scientific impact in a field outside their original scope. We discovered examples of coordinated mechanisms of viral gene control through the combined analysis of nucleosome occupancy, histone modification patterning, combinatorial transcription factor binding, and long-range DNA looping. Several of these mechanisms are reminiscent of those in the human genome and illustrate the functional similarity of a virus and its host.

We provide insights into host-virus interactions through combined genome-wide expression analyses. We aggregated hundreds of RNA-seq experiments and observed many cell lines displaying surprisingly high levels of early lytic-cycle genes relative to late lytic-cycle genes. The correlation of this gene expression program with EBV copy number suggests that abortive lytic DNA replication may be an important mechanism for viral genome maintenance and host cell population fitness. Furthermore, analyses of virus and host transcriptomes revealed unexpected coordination between viral lytic reactivation and cellular pathways involved in B cell expansion and tumor promotion. These findings are consistent with studies showing that viral lytic-cycle gene expression correlates with EBV carcinogenesis in humans (Dardari et al., 2000; Hanto et al., 1983) and contributes to lymphomagenesis in a humanized mouse model (Ma et al., 2011).

We also examine host-virus interactions at individual regulatory loci and provide insights into the relationship between chromatin organization, gene regulation, and how developmental regulatory factors link these processes. The B cell identity factor Pax5 was found to bind within the viral terminal repeats and modulate transcription of viral oncogenes from within the DNA loop connecting CTCF-cohesin peaks at LMP1 and OriP loci. These binding sites are reminiscent of a similar coordination of Pax5 and CTCF sites identified within the IgG locus, which function to direct class switching during B cell maturation (Ebert et al., 2011). Pax5 mutations have been implicated in B cell lymphomagenesis, which may result in dysregulation of LMP expression in certain EBV malignancies, including Hodgkins's disease (McCune et al., 2006; Pasqualucci et al., 2001). Additionally, downregulation of Pax5 during typical germinal center reaction may derepress LMP1 and LMP2, providing a mechanism for virus-mediated rescue from apoptosis of somatically hypermutated B cells that harbor tumorigenic translocations so commonly seen in EBV-associated malignancies (Bechtel et al., 2005; Klein and Dalla-Favera, 2008; Mancao et al., 2005; Roughan and Thorley-Lawson, 2009). These observations suggest that breakdown of host regulatory pathways for controlling EBV gene expression may contribute to tumorigenesis through dysregulation of viral oncogenes.

EBV was discovered as the first human tumor virus nearly 50 years ago and was among the first genomes sequenced. It is thus fitting that it serves as the prototype for functional genomic and epigenomic elements in a human tumor virus, providing a foundation for future work in viral genomics and the emerging field of systems virology (Peng et al., 2009). We anticipate that system-level and data-driven approaches will ultimately lead to more comprehensive models of viral persistence and its role in human cellular development and oncogenesis.

EXPERIMENTAL PROCEDURES

Aligning Reads to the Viral and Host Genomes

Data was aggregated from a variety of sources (Table S1) and aligned to the EBV genome (GenBank accession number NC_007605, March 2010) using the Bowtie program allowing for one mismatch. We ignore all reads that aligned to the human genome, which ensured that all EBV reads are uniquely EBV and not actually from similar host sequence. To subtract human reads, we mapped all reads to hg19 (including all "Un" and "random" chromosomes), using the same parameters as when aligning to the viral genome. The subtraction of human-aligning reads resulted in small regions of the EBV-genome becoming unmappable (Figure S1).

Analysis of Transcription Factor Binding Sites

Transcription factor ChIP-seq peaks with significantly more reads than IgG and input control sequencing experiments were identified. We modeled reads in the control experiments by a Poisson distribution, and a p value of 1.72×10^{-7} was used as a cutoff for peak calling, which represents a genome-wide familywise error rate of 0.01. Validation of a subset of ChIP-seq peaks was performed as previously described (Tempera et al., 2010). In brief, cells were fixed in 1% formaldehyde for 30 min, and DNA was sonicated to between 200 and 350 base pairs. ChIP DNA was amplified on an ABI Prism 7000 using SYBR green chemistry.

Estimation of Viral and Human Gene Expression

TopHat and Cufflinks were used to align reads and quantify known transcripts (Trapnell et al., 2010). Transcript abundances were normalized by reads per kilobase per million (RPKM). Human transcripts were taken from RefSeq annotations for hg19. Multimapping reads were allowed to map to 30 regions in the transcriptome before being ignored. RPKM values were normalized to account for multimapping reads. Gene abundance was estimated as the sum of all transcript isoforms. The per-million normalization was done relative only to reads mapping to EBV or human, since this ensured independence of transcript quantification in EBV and human. Use of absolute transcript quantities (normalized to total alignable reads in both EBV and human) is used only when noted. RNA-seq experiments with low read count (less than 1 million alignable human reads) samples were removed, and technical replicates were averaged. From the original 294 RNA-seq assays, we obtained 201 reliable and independent samples.

Chromatin Conformation Capture

Chromatin conformation capture was performed as previously described (Hagège et al., 2007; Tempera et al., 2011) with minor modifications. In brief, cells were put through a 70 μm filter to obtain single cells. Ten million cells were fixed in 1% formaldehyde for 30 min, and the reaction was quenched with 0.125 M glycine. Cells were centrifuged, resuspended in lysis buffer, and lysed for 10 min. Nuclei were collected and digested with 500 U MseI restriction enzyme overnight at 37°C. The digestion was halted by incubation at 65°C in 1.6% SDS on a 1,200 RPM shaker. The sample was diluted 10-fold, followed by ligation reaction containing 100 U T4 DNA ligase for 4 hr at 16°C and 45 min at room temperature. The sample was digested by 300 μg proteinase K at 65°C overnight, followed by RNase treatment for 1 hr at 37°C. DNA was phenol-chloroform extracted and ethanol precipitated and analyzed with PCR, qPCR, and sequencing. As a control, the EBV bacmid was MseI digested and ligated, thus creating all possible ligation products at background concentrations.

Micrococcal Nuclease Digestion

Nuclei were isolated from 5×10^7 Mutu and Mutu-LCL cells with a Dounce homogenizer in 4 ml lysis buffer (0.3 M sucrose, 2 mM magnesium acetate,

3 mM CaCl2, 1% Triton X-100, and 10 mM HEPES [pH 7.9]). The lysate was centrifuged through a glycerol cushion (25% glycerol, 5 mM magnesium acetate, 0.1 mM EDTA, and 10 mM HEPES [pH 7.4]) at 1,000 g for 15 min at 4°C. The nuclei were incubated with micrococal nuclease I (500 U/ml) at 37°C for 20 min in 200 μl digestion buffer (25 mM KCl, 4 mM MgCl2, 1 mM CaCl2, 50 mM Tris [pH 7.4], and 12.5% glycerol). The reaction was stopped by equal volume of stop buffer (2% SDS, 0.2 M NaCl, 10 mM EDTA, 10 mM EGTA, 50 mM Tris [pH 8.0], and proteinase K [100 μg/ml]) for 2 hr at 50°C. Micrococcal nuclease I (MNase I) resistant DNA was extracted by phenol-chloroform and ethanol precipitation. The ~150 bp mononucleosomal DNA was isolated from 1.5% agarose gel and purified by the QIAquick Gel extraction kit (QIAGEN) according to the manufacturer's protocol. Purified DNA was then subject to Solexa sequencing according to the manufacturer's recommendations (Illumina).

Lentiviral Delivery of shRNA

Lentiviral shRNAs were obtained from the Sigma-Aldrich MISSION shRNA library. Four million Mutu-LCL cells were passed through a 40 μm filter, spun down, and resuspended in 2 ml lentivirus suspension. Cells were spun at 500 g for 90 min at 25°C. Cell were cultured at ~500,000 cells/ml for 5 days with media changes in 1 μg/ml puromycin. Knockdown was confirmed by western blot and qRT-PCR.

Pulsed-Field Gel Electrophoresis

For resolution of large viral genomic DNA fragments, PFGE was performed as described previously (Dheekollu and Lieberman, 2011). In brief, DNA migrated for a duration of 23 hr at 14°C with the pulse ramping linearly every 60–120 s through 120°C using a Bio-Rad CHEF Mapper.

ACCESSION NUMBERS

Data generated by our lab have been submitted to NCBI GEO under accession numbers GSE30709 and GSE39913.

SUPPLEMENTAL INFORMATION

Supplemental Information includes ten tables, six figures, and Supplemental Experimental Procedures and can be found with this article online at http://dx.doi.org/10.1016/j.chom.2012.06.008.

ACKNOWLEDGMENTS

This work was supported by funds from NIH awards CA085678, CA093606, and DE017336 to P.M.L., NIH award HG006798 to C.L., and a K99AI099153 award from the National Institute of Allergy and Infectious Diseases to I.T. We thank Dr. Louise Showe and Priyankara Wikramasinghe from the Wistar Institute Genomics and Bioinformatics facilities and acknowledge the support of the Wistar Institute Cancer Center Core grant P30 CA10815. We also thank Chris Wawak and Joanne Edington for technical support.

Received: August 9, 2011
Revised: April 13, 2012
Accepted: June 1, 2012
Published: August 15, 2012

REFERENCES

Aderem, A., Adkins, J.N., Ansong, C., Galagan, J., Kaiser, S., Korth, M.J., Law, G.L., McDermott, J.G., Proll, S.C., Rosenberger, C., et al. (2011). A systems biology approach to infectious disease research: innovating the pathogen-host research paradigm. MBio *2*, e00325–e10.

Altshuler, D.M., Gibbs, R.A., Peltonen, L., Altshuler, D.M., Gibbs, R.A., Peltonen, L., Dermitzakis, E., Schaffner, S.F., Yu, F., Peltonen, L., et al; International HapMap 3 Consortium. (2010). Integrating common and rare genetic variation in diverse human populations. Nature *467*, 52–58.

Ascherio, A., and Munger, K.L. (2010). Epstein-Barr virus infection and multiple sclerosis: a review. J. Neuroimmune Pharmacol. *5*, 271–277.

Austin, P.J., Flemington, E., Yandava, C.N., Strominger, J.L., and Speck, S.H. (1988). Complex transcription of the Epstein-Barr virus BamHI fragment H rightward open reading frame 1 (BHRF1) in latently and lytically infected B lymphocytes. Proc. Natl. Acad. Sci. USA *85*, 3678–3682.

Bechtel, D., Kurth, J., Unkel, C., and Küppers, R. (2005). Transformation of BCR-deficient germinal-center B cells by EBV supports a major role of the virus in the pathogenesis of Hodgkin and posttransplantation lymphomas. Blood *106*, 4345–4350.

Bergbauer, M., Kalla, M., Schmeinck, A., Göbel, C., Rothbauer, U., Eck, S., Benet-Pagès, A., Strom, T.M., and Hammerschmidt, W. (2010). CpG-methylation regulates a class of Epstein-Barr virus promoters. PLoS Pathog. *6*, e1001114.

Birney, E., Stamatoyannopoulos, J.A., Dutta, A., Guigó, R., Gingeras, T.R., Margulies, E.H., Weng, Z., Snyder, M., Dermitzakis, E.T., Thurman, R.E., et al; ENCODE Project Consortium; NISC Comparative Sequencing Program; Baylor College of Medicine Human Genome Sequencing Center; Washington University Genome Sequencing Center; Broad Institute; Children's Hospital Oakland Research Institute. (2007). Identification and analysis of functional elements in 1% of the human genome by the ENCODE pilot project. Nature *447*, 799–816.

Breitbart, M., Hewson, I., Felts, B., Mahaffy, J.M., Nulton, J., Salamon, P., and Rohwer, F. (2003). Metagenomic analyses of an uncultured viral community from human feces. J. Bacteriol. *185*, 6220–6223.

Calderwood, M.A., Venkatesan, K., Xing, L., Chase, M.R., Vazquez, A., Holthaus, A.M., Ewence, A.E., Li, N., Hirozane-Kishikawa, T., Hill, D.E., et al. (2007). Epstein-Barr virus and virus human protein interaction maps. Proc. Natl. Acad. Sci. USA *104*, 7606–7611.

Cheung, V.G., Nayak, R.R., Wang, I.X., Elwyn, S., Cousins, S.M., Morley, M., and Spielman, R.S. (2010). Polymorphic cis- and trans-regulation of human gene expression. PLoS Biol. *8*, e1000480.

Choy, E., Yelensky, R., Bonakdar, S., Plenge, R.M., Saxena, R., De Jager, P.L., Shaw, S.Y., Wolfish, C.S., Slavik, J.M., Cotsapas, C., et al. (2008). Genetic analysis of human traits in vitro: drug response and gene expression in lymphoblastoid cell lines. PLoS Genet. *4*, e1000287.

Dardari, R., Khyatti, M., Benider, A., Jouhadi, H., Kahlain, A., Cochet, C., Mansouri, A., El Gueddari, B., Benslimane, A., and Joab, I. (2000). Antibodies to the Epstein-Barr virus transactivator protein (ZEBRA) as a valuable biomarker in young patients with nasopharyngeal carcinoma. Int. J. Cancer *86*, 71–75.

Davies, M.L., Xu, S., Lyons-Weiler, J., Rosendorff, A., Webber, S.A., Wasil, L.R., Metes, D., and Rowe, D.T. (2010). Cellular factors associated with latency and spontaneous Epstein-Barr virus reactivation in B-lymphoblastoid cell lines. Virology *400*, 53–67.

Dheekollu, J., and Lieberman, P.M. (2011). The replisome pausing factor Timeless is required for episomal maintenance of latent Epstein-Barr virus. J. Virol. *85*, 5853–5863.

Dresang, L.R., Vereide, D.T., and Sugden, B. (2009). Identifying sites bound by Epstein-Barr virus nuclear antigen 1 (EBNA1) in the human genome: defining a position-weighted matrix to predict sites bound by EBNA1 in viral genomes. J. Virol. *83*, 2930–2940.

Dyer, M.D., Murali, T.M., and Sobral, B.W. (2008). The landscape of human proteins interacting with viruses and other pathogens. PLoS Pathog. *4*, e32.

Ebert, A., McManus, S., Tagoh, H., Medvedovic, J., Salvagiotto, G., Novatchkova, M., Tamir, I., Sommer, A., Jaritz, M., and Busslinger, M. (2011). The distal V(H) gene cluster of the *Igh* locus contains distinct regulatory elements with Pax5 transcription factor-dependent activity in pro-B cells. Immunity *34*, 175–187.

Feng, H., Shuda, M., Chang, Y., and Moore, P.S. (2008). Clonal integration of a polyomavirus in human Merkel cell carcinoma. Science *319*, 1096–1100.

Gahn, T.A., and Sugden, B. (1995). An EBNA-1-dependent enhancer acts from a distance of 10 kilobase pairs to increase expression of the Epstein-Barr virus LMP gene. J. Virol. *69*, 2633–2636.

Gerstein, M.B., Lu, Z.J., Van Nostrand, E.L., Cheng, C., Arshinoff, B.I., Liu, T., Yip, K.Y., Robilotto, R., Rechtsteiner, A., Ikegami, K., et al; modENCODE

Consortium. (2010). Integrative analysis of the Caenorhabditis elegans genome by the modENCODE project. Science *330*, 1775–1787.

Glaser, R., Tarr, K.L., and Dangel, A.W. (1989). The transforming prototype of Epstein-Barr virus (B95-8) is also a lytic virus. Int. J. Cancer *44*, 95–100.

Günther, T., and Grundhoff, A. (2010). The epigenetic landscape of latent Kaposi sarcoma-associated herpesvirus genomes. PLoS Pathog. *6*, e1000935.

Hagège, H., Klous, P., Braem, C., Splinter, E., Dekker, J., Cathala, G., de Laat, W., and Forné, T. (2007). Quantitative analysis of chromosome conformation capture assays (3C-qPCR). Nat. Protoc. *2*, 1722–1733.

Hanto, D.W., Gajl-Peczalska, K.J., Frizzera, G., Arthur, D.C., Balfour, H.H., Jr., McClain, K., Simmons, R.L., and Najarian, J.S. (1983). Epstein-Barr virus (EBV) induced polyclonal and monoclonal B-cell lymphoproliferative diseases occurring after renal transplantation. Clinical, pathologic, and virologic findings and implications for therapy. Ann. Surg. *198*, 356–369.

Hutzinger, R., Feederle, R., Mrazek, J., Schiefermeier, N., Balwierz, P.J., Zavolan, M., Polacek, N., Delecluse, H.-J., and Hüttenhofer, A. (2009). Expression and processing of a small nucleolar RNA from the Epstein-Barr virus genome. PLoS Pathog. *5*, e1000547.

Iizasa, H., Wulff, B.-E., Alla, N.R., Maragkakis, M., Megraw, M., Hatzigeorgiou, A., Iwakiri, D., Takada, K., Wiedmer, A., Showe, L., et al. (2010). Editing of Epstein-Barr virus-encoded BART6 microRNAs controls their dicer targeting and consequently affects viral latency. J. Biol. Chem. *285*, 33358–33370.

Iyer, L.M., Balaji, S., Koonin, E.V., and Aravind, L. (2006). Evolutionary genomics of nucleo-cytoplasmic large DNA viruses. Virus Res. *117*, 156–184.

Kasowski, M., Grubert, F., Heffelfinger, C., Hariharan, M., Asabere, A., Waszak, S.M., Habegger, L., Rozowsky, J., Shi, M., Urban, A.E., et al. (2010). Variation in transcription factor binding among humans. Science *328*, 232–235.

Kelly, G.L., Long, H.M., Stylianou, J., Thomas, W.A., Leese, A., Bell, A.I., Bornkamm, G.W., Mautner, J., Rickinson, A.B., and Rowe, M. (2009). An Epstein-Barr virus anti-apoptotic protein constitutively expressed in transformed cells and implicated in Burkitt lymphomagenesis: the Wp/BHRF1 link. PLoS Pathog. *5*, e1000341.

Klein, U., and Dalla-Favera, R. (2008). Germinal centres: role in B-cell physiology and malignancy. Nat. Rev. Immunol. *8*, 22–33.

Lee, B.-K., Bhinge, A.A., and Iyer, V.R. (2011). Wide-ranging functions of E2F4 in transcriptional activation and repression revealed by genome-wide analysis. Nucleic Acids Res. *39*, 3558–3573.

Li, M., Wang, I.X., Li, Y., Bruzel, A., Richards, A.L., Toung, J.M., and Cheung, V.G. (2011). Widespread RNA and DNA sequence differences in the human transcriptome. Science *333*, 53–58.

Lieberman, P.M. (2006). Chromatin regulation of virus infection. Trends Microbiol. *14*, 132–140.

Lin, Z., Xu, G., Deng, N., Taylor, C., Zhu, D., and Flemington, E.K. (2010). Quantitative and qualitative RNA-Seq-based evaluation of Epstein-Barr virus transcription in type I latency Burkitt's lymphoma cells. J. Virol. *84*, 13053–13058.

Lindner, S.E., and Sugden, B. (2007). The plasmid replicon of Epstein-Barr virus: mechanistic insights into efficient, licensed, extrachromosomal replication in human cells. Plasmid *58*, 1–12.

Lu, D., Zhao, Y., Tawatao, R., Cottam, H.B., Sen, M., Leoni, L.M., Kipps, T.J., Corr, M., and Carson, D.A. (2004). Activation of the Wnt signaling pathway in chronic lymphocytic leukemia. Proc. Natl. Acad. Sci. USA *101*, 3118–3123.

Lu, F., Wikramasinghe, P., Norseen, J., Tsai, K., Wang, P., Showe, L., Davuluri, R.V., and Lieberman, P.M. (2010). Genome-wide analysis of host-chromosome binding sites for Epstein-Barr Virus Nuclear Antigen 1 (EBNA1). Virol. J. *7*, 262.

Ma, S.-D., Hegde, S., Young, K.H., Sullivan, R., Rajesh, D., Zhou, Y., Jankowska-Gan, E., Burlingham, W.J., Sun, X., Gulley, M.L., et al. (2011). A new model of Epstein-Barr virus infection reveals an important role for early lytic viral protein expression in the development of lymphomas. J. Virol. *85*, 165–177.

Mancao, C., Altmann, M., Jungnickel, B., and Hammerschmidt, W. (2005). Rescue of "crippled" germinal center B cells from apoptosis by Epstein-Barr virus. Blood *106*, 4339–4344.

McCune, R.C., Syrbu, S.I., and Vasef, M.A. (2006). Expression profiling of transcription factors Pax-5, Oct-1, Oct-2, BOB.1, and PU.1 in Hodgkin's and non-Hodgkin's lymphomas: a comparative study using high throughput tissue microarrays. Mod. Pathol. *19*, 1010–1018.

Montgomery, S.B., Sammeth, M., Gutierrez-Arcelus, M., Lach, R.P., Ingle, C., Nisbett, J., Guigo, R., and Dermitzakis, E.T. (2010). Transcriptome genetics using second generation sequencing in a Caucasian population. Nature *464*, 773–777.

Moore, P.S., and Chang, Y. (2010). Why do viruses cause cancer? Highlights of the first century of human tumour virology. Nat. Rev. Cancer *10*, 878–889.

Moorman, C., Sun, L.V., Wang, J., de Wit, E., Talhout, W., Ward, L.D., Greil, F., Lu, X.J., White, K.P., Bussemaker, H.J., and van Steensel, B. (2006). Hotspots of transcription factor colocalization in the genome of Drosophila melanogaster. Proc. Natl. Acad. Sci. USA *103*, 12027–12032.

Parkin, D.M. (2006). The global health burden of infection-associated cancers in the year 2002. Int. J. Cancer *118*, 3030–3044.

Pasqualucci, L., Neumeister, P., Goossens, T., Nanjangud, G., Chaganti, R.S., Küppers, R., and Dalla-Favera, R. (2001). Hypermutation of multiple proto-oncogenes in B-cell diffuse large-cell lymphomas. Nature *412*, 341–346.

Peng, X., Chan, E.Y., Li, Y., Diamond, D.L., Korth, M.J., and Katze, M.G. (2009). Virus-host interactions: from systems biology to translational research. Curr. Opin. Microbiol. *12*, 432–438.

Pickrell, J.K., Marioni, J.C., Pai, A.A., Degner, J.F., Engelhardt, B.E., Nkadori, E., Veyrieras, J.-B., Stephens, M., Gilad, Y., and Pritchard, J.K. (2010). Understanding mechanisms underlying human gene expression variation with RNA sequencing. Nature *464*, 768–772.

Pinney, J.W., Dickerson, J.E., Fu, W., Sanders-Beer, B.E., Ptak, R.G., and Robertson, D.L. (2009). HIV-host interactions: a map of viral perturbation of the host system. AIDS *23*, 549–554.

Ramagopalan, S.V., Heger, A., Berlanga, A.J., Maugeri, N.J., Lincoln, M.R., Burrell, A., Handunnetthi, L., Handel, A.E., Disanto, G., Orton, S.-M., et al. (2010). A ChIP-seq defined genome-wide map of vitamin D receptor binding: associations with disease and evolution. Genome Res. *20*, 1352–1360.

Rennekamp, A.J., and Lieberman, P.M. (2011). Initiation of Epstein-Barr virus lytic replication requires transcription and the formation of a stable RNA-DNA hybrid molecule at OriLyt. J. Virol. *85*, 2837–2850.

Repic, A.M., Shi, M., Scott, R.S., and Sixbey, J.W. (2010). Augmented latent membrane protein 1 expression from Epstein-Barr virus episomes with minimal terminal repeats. J. Virol. *84*, 2236–2244.

Reyes, A., Haynes, M., Hanson, N., Angly, F.E., Heath, A.C., Rohwer, F., and Gordon, J.I. (2010). Viruses in the faecal microbiota of monozygotic twins and their mothers. Nature *466*, 334–338.

Rickinson, A.B., and Kieff, E. (2007). Epstein-Barr virus, D.M. Knipe and P.M. Howley, eds. (Philadelphia, PA: Lippincott Williams & Wilkins), pp. 2655–2700.

Roughan, J.E., and Thorley-Lawson, D.A. (2009). The intersection of Epstein-Barr virus with the germinal center. J. Virol. *83*, 3968–3976.

Roy, S., Ernst, J., Kharchenko, P.V., Kheradpour, P., Negre, N., Eaton, M.L., Landolin, J.M., Bristow, C.A., Ma, L., Lin, M.F., et al; modENCODE Consortium. (2010). Identification of functional elements and regulatory circuits by Drosophila modENCODE. Science *330*, 1787–1797.

Sjöblom, A., Jansson, A., Yang, W., Laín, S., Nilsson, T., and Rymo, L. (1995). PU box-binding transcription factors and a POU domain protein cooperate in the Epstein-Barr virus (EBV) nuclear antigen 2-induced transactivation of the EBV latent membrane protein 1 promoter. J. Gen. Virol. *76*, 2679–2692.

Stedman, W., Kang, H., Lin, S., Kissil, J.L., Bartolomei, M.S., and Lieberman, P.M. (2008). Cohesins localize with CTCF at the KSHV latency control region and at cellular c-myc and H19/Igf2 insulators. EMBO J. *27*, 654–666.

Subramanian, A., Tamayo, P., Mootha, V.K., Mukherjee, S., Ebert, B.L., Gillette, M.A., Paulovich, A., Pomeroy, S.L., Golub, T.R., Lander, E.S., and Mesirov, J.P. (2005). Gene set enrichment analysis: a knowledge-based

approach for interpreting genome-wide expression profiles. Proc. Natl. Acad. Sci. USA *102*, 15545–15550.

Tadmor, A.D., Ottesen, E.A., Leadbetter, J.R., and Phillips, R. (2011). Probing individual environmental bacteria for viruses by using microfluidic digital PCR. Science *333*, 58–62.

Tempera, I., Wiedmer, A., Dheekollu, J., and Lieberman, P.M. (2010). CTCF prevents the epigenetic drift of EBV latency promoter Qp. PLoS Pathog. *6*, e1001048.

Tempera, I., Klichinsky, M., and Lieberman, P.M. (2011). EBV latency types adopt alternative chromatin conformations. PLoS Pathogens *7*, e1002180.

Thorley-Lawson, D.A., and Gross, A. (2004). Persistence of the Epstein-Barr virus and the origins of associated lymphomas. N. Engl. J. Med. *350*, 1328–1337.

Tierney, R., Kirby, H., Nagra, J., Rickinson, A., and Bell, A. (2000). The Epstein-Barr virus promoter initiating B-cell transformation is activated by RFX proteins and the B-cell-specific activator protein BSAP/Pax5. J. Virol. *74*, 10458–10467.

Tierney, R., Nagra, J., Hutchings, I., Shannon-Lowe, C., Altmann, M., Hammerschmidt, W., Rickinson, A., and Bell, A. (2007). Epstein-Barr virus exploits BSAP/Pax5 to achieve the B-cell specificity of its growth-transforming program. J. Virol. *81*, 10092–10100.

Toth, Z., Maglinte, D.T., Lee, S.H., Lee, H.-R., Wong, L.-Y., Brulois, K.F., Lee, S., Buckley, J.D., Laird, P.W., Marquez, V.E., and Jung, J.U. (2010). Epigenetic analysis of KSHV latent and lytic genomes. PLoS Pathog. *6*, e1001013.

Trapnell, C., Williams, B.A., Pertea, G., Mortazavi, A., Kwan, G., van Baren, M.J., Salzberg, S.L., Wold, B.J., and Pachter, L. (2010). Transcript assembly and quantification by RNA-Seq reveals unannotated transcripts and isoform switching during cell differentiation. Nat. Biotechnol. *28*, 511–515.

Xu, G., Fewell, C., Taylor, C., Deng, N., Hedges, D., Wang, X., Zhang, K., Lacey, M., Zhang, H., Yin, Q., et al. (2010). Transcriptome and targetome analysis in MIR155 expressing cells using RNA-seq. RNA *16*, 1610–1622.

Young, L.S., and Rickinson, A.B. (2004). Epstein-Barr virus: 40 years on. Nat. Rev. Cancer *4*, 757–768.

Zhou, J., Chau, C.M., Deng, Z., Shiekhattar, R., Spindler, M.-P., Schepers, A., and Lieberman, P.M. (2005). Cell cycle regulation of chromatin at an origin of DNA replication. EMBO J. *24*, 1406–1417.